Quaternary International 580 (2021) 22–37

Contents lists available at ScienceDirect

Quaternary International

journal homepage: www.elsevier.com/locate/quaint

# Late Quaternary episodes of clastic sediment deposition in the Tarimba Cave, Central Brazil

Dandara Caldeira [a,*], Rogério Uagoda [a,b], Adivane Morais Nogueira [b], Jeremie Garnier [a], André Oliveira Sawakuchi [c], Yawar Hussain [d]

[a] Institute of Geoscience, University of Brasilia, Brasilia, 70910-900, Brazil
[b] Department of Geography, University of Brasilia, Brasilia, 70910-900, Brazil
[c] Institute of Geosciences, University of São Paulo, São Paulo, 05508-080, Brazil
[d] Department of Geology, Liège University, Liège, 4032, Belgium

ARTICLE INFO

*Keywords:*
Cave
Paleoenvironment
Sedimentation
Sedimentary facies

ABSTRACT

The study presents three sedimentary profiles from Tarimba cave in central Brazil. The data allow constraining the late Quaternary sedimentary evolution of cave systems in the region. A multi-techniques approach was used to characterize sediment texture (grain size and circularity index), mineralogical composition (X-Ray Diffraction), chemical composition (ICP-OES) and deposition ages (Optically Stimulated Luminescence and radiocarbon). Eight sedimentary facies were identified, including a facies formed by autochthonous sediments (Guano) and seven facies formed by allochthonous siliciclastic sediments. The siliciclastic facies range from clayey to gravelly deposits that correspond to high-density gravity flows (Diamicton) and water laid traction process of varied deposition energy (Channel, Backswamp, and Slackwater). The studied deposits reflect an intense cave filing from the Middle to Late Pleistocene in the last 200 Ka. Subsequent depositional events formed three sedimentation phases: the first before 200 Ka corresponding to a larger granulometric interval, clay to gravel, identified through erosive surfaces; the second, after 197 Ka, is composed of sandy sediments and oscillations in the water flow energy. The third phase between 87 and 52 Ka (which covered the other stages) was responsible for the last fluvial deposition.

## 1. Introduction

Caves are fragile systems that may contain and preserve reliable sedimentary records of surface and subsurface paleoenvironmental conditions. The allochthonous (clastic) and autochthonous (chemical or biogenic) sediments deposited within caves, which provide a degree of resilience to physical and chemical weathering process and erosion, providing unique paleoenvironmental records for the Quaternary deposits (Gillieson, 1996; Ballesteros et al., 2019; McAdams et al., 2019). Although the sedimentation processes inside a cave are analogous to the surface ones, they are poorly documented in comparison with surface systems and their complex depositional-erosive dynamics, often difficult their paleoenvironmental significance (Gillieson, 1996; White, 2007). Moreover, cave sedimentary systems are coupled to surface conditions and their understanding needs a comprehensive and diverse knowledge derived from geomorphologic, sedimentological, paleo-ecological, and geochronological studies compared to external records (Woodward and Goldberg, 2001).

Generally, the clastic sediments within caves are allochthonous and derived from adjacent rocks units under weathering, and their triggers mechanism depends on external regional factors such as climate, tectonics and surface geomorphology, thus representing the scenario of the surrounding environment/watershed (Farrant and Smart, 2011; Plotnick et al., 2015). Therefore, the deposited materials and deposition patterns reflect the scale of terrestrial processes caused by regional driving forces transmitted by climate and tectonics (Springer, 2005; Arriolabengoa et al., 2015).

The study of clastic sediments in caves is challenging since even with deposition processes similar to the superficial ones, the particular sedimentary dynamics in the cave can lead to deposits with complex stratigraphic configurations (Osborne, 1986; Gillieson, 1996; Ford and Williams, 2007), sometimes having older sediments overlapping the younger ones (Springer, 2005). Moreover, the deposition in the conduits is highly heterogeneous, generating temporal gaps and discontinuity

* Corresponding author.
*E-mail address:* dandara.caldeira2014@gmail.com (D. Caldeira).

https://doi.org/10.1016/j.quaint.2021.01.012
Received 14 November 2020; Received in revised form 12 January 2021; Accepted 15 January 2021
Available online 20 January 2021

into sediment records, reinforcing the need to gather several deposits to obtain a more comprehensive paleoenvironmental scenario (Gillieson, 1996; Plotnick et al., 2015). Thus, establishing a precise chronology of depositional and erosion phases is fundamental to shed light on the connections between underground and surface events (Osborne, 2005; White, 2007).

In this context, Brazil stands out for presenting expressive cave systems with more than 20,000 mapped caves and a growing potential for increase (ICMBio/CECAV, 2020). In the last decades, clastic sediments within caves have been consolidated as an important target to reconstruct paleoenvironmental conditions of both surface and subsurface landscapes since this is a crucial demand for extensive paleontological and/or archaeological studies performed so far (Roosevelt et al., 1996; Michab et al., 1998; Peyre et al., 1998; Faure et al., 1999; Santos et al., 2003; Piló et al., 2005; Auler et al., 2006; Fontugne, 2013; Kinoshita et al., 2014; Oliveira et al., 2014). Among the studies about Brazilian cave deposits (Auler et al., 2002, 2009; Hubbe et al., 2011; Jaqueto et al., 2016; Laureano et al., 2016; Haddad-Martim et al., 2017; Novello et al., 2019), few of them have been carried out in the central region of the country (Auler et al., 2002; Jaqueto et al., 2016) and so far there are no studies about sedimentary deposits within caves from on the western edge of the São Francisco Craton, which hosts a major Brazilian karst area.

The state of Goiás is the 5th largest in the number of mapped caves in Brazil, hosting approximately 1001 cavities, among them the Tarimba cave. Tarimba is the significant cave of Vermelho River Rising Environmental Protection Area (APARNRV), in central Brazil (Fig. 1), being the sixth largest cave in horizontal projection of the Brazilian territory with about 14 km mapped, but still little studied. It holds an endemic fauna and is currently threatened by anthropic activities. On all over the APARNRV there are anthropogenic activities with potential for environmental impacts, such as the use of cave waters for public supply,

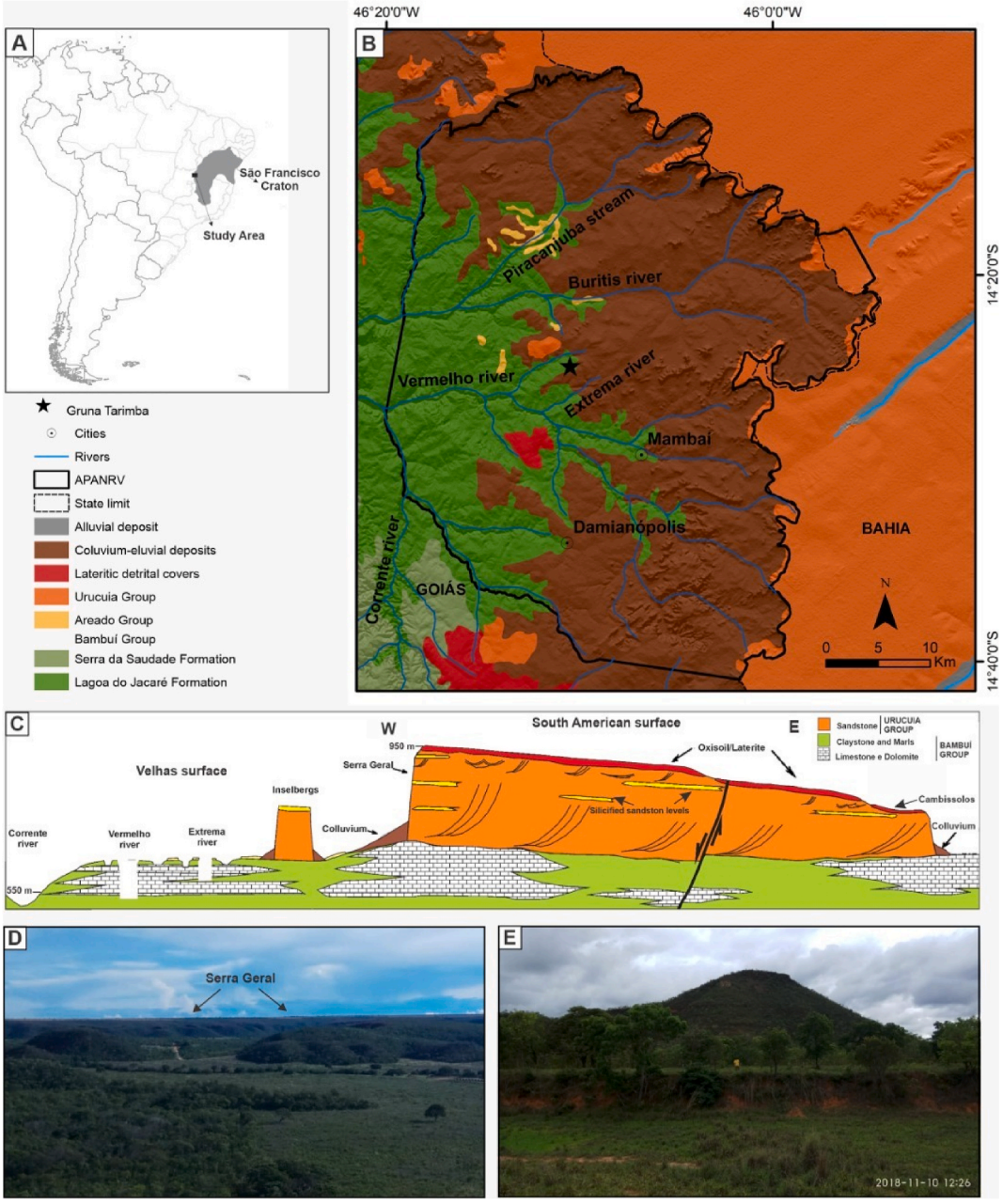


**Fig. 1.** Location of the study area in the São Francisco Craton. B- Geological map. Source: Serviço Geológico do Brasil (CPRM). Coordinate system, UTM. Zone, 23S. SIRGAS 2000. C - Geomorphological context (Gaspar and Campos, 2007) adapted by Uagoda et al. (2019). D - Serra Geral overview. E– Inserlberg near carbonates.

mining in karstic areas, severe soil degradation, sedimentation in recharging areas and accelerated pipeline clogging (ICMBio/CECAV, 2017). This work aims to understand the sedimentary dynamics within the Tarimba cave during the late Quaternary, including the association of the surrounding surface landscape's evolution dynamics. Also, it seeks to provide the first composition characterization and chronology of deposition of clastic sediments in the region that may serve as a basis for paleoenvironmental interpretations.

## 2. Geological/geomorphological context

The study area is located on the western edge of the São Francisco Craton, being composed of sediments of the São Francisco Basin (Fig. 1-A). The base, formed by a succession of carbonate and silicaceous rocks of the Neoproterozoic Bambuí Group, hosts one of Brazil's main karst provinces. The carbonated succession is covered by Phanerozoic sediments of the Sanfranciscan Basin (Areado Group, Urucuia Group, and Chapadão Formation) (Campos and Dardenne, 1997), Fig. 1-B.

The Bambuí Group occurs extensively in the area and is associated with sediment deposition on a stable epicontinental platform from transgressive-regressive mega-cycles in a basin with a very low bottom gradient and shallow waters (Dardenne et al., 1978; Dardenne, 1981; Araujo and Moreton, 2008). In the area, the total thickness of the complete stratigraphy is 1700 m (Cruz, 2012) include six lithostratigraphic formations, proposed by Dardenne et al. (1978), described from the base to the top as: Jequitaí Formation, Sete Lagoas Formation, Serra de Santa Helena Formation, Lagoa do Jacaré Formation, Serra da Saudade Formation, and Três Marias Formation. Locally, the Lagoa do Jacaré Formation is characterized by the intercalation of oolitic and pisolitic limestones, dark grey, foul, crystalline, lenticular with siltstones and marls. It constitutes the predominant lithology of the region and where the caves are developed, including Tarimba cave.

The Areado Group occurs only in the northern portion and corresponds to sediments of the Eocretaceous marked by lateral variations due to the various depositional environments (Campos and Dardenne, 1997). The Urucuia Group has Cretaceous ages and consists basically of sandstones in a system of fluvial/eolic deposition occurring in the eastern portion of the area, primarily in the state of Bahia and in some inselbergs near the carbonates. The Urucuia Group is characterized by quartz sandstones, reddish and white, fine to medium grain, rounded and well-selected with rare occurrence of clay matrix (Iglesias and Uhlein, 2009). Locally the pink to reddish sandstones, thin to medium, develop in the form of isolated inselbergs (Cruz, 2012). The sandstone forms a reddish well developed oxisol and sometimes forms lateritics outcrops on the surface (Fig. 1A and B). The Chapadão Formation expressively occurs in the region corresponding to the Cenozoic colluvium/detritic covers, predominantly unconsolidated sandy. The formation results from intense processes of erosion and escarpment regression of Ucucuia group, forming Talus deposits and covering the formations from Bambuí group where the caves are located (Campos and Dardenne, 1997; Iglesias and Uhlein, 2009).

The geomorphological configuration is a cuesta landscape called Serra Geral de Goiás, generated mainly by regressive erosion (Cherem and Varajão, 2014), Figs. 1-C and 1-D. The mountain range has a north-south direction with about 400 km of extension is the divider of two important Brazilian watersheds, São Francisco (east) and Tocantins-Araguaia (west). In this scenario, the upper portion (Chapadão Central), remaining from the South American surface, makes up the sandstones of the Urucuia Group. The lower portion (Vão do Paranã) corresponds to the remnants of the Velhas surface installed in the rocks of the Bambui Group. In the intermediate portions are observed colluvium-eluvial deposits generated by the sandstone's erosion (Cherem and Varajão, 2014). The area is still observed inselberg hills that stand out in the middle of the landscape (Fig. 1– E).

Erosive processes involving the Chapadão Central retreat remove sediments and leave them available in hillslopes to later transportation to the underground karstic system located downstream.

Such dynamics favor a covered karstic system in which two types of caves stand out: those near the transition zone between karstic lands and talus (alluvial-colluvial deposits from the Urucuia Group) with vadose and meandering caves filled by sediments and signs of paragenesis; and those fluvial caves adjusted to the rivers inside canyons are transporting the fluvial load. (Hussain and Uagoda, 2021).

The evolution of karst correlates with local rivers dynamics such as Vermelho, Buritis, Piracanjuba, and Prata was developed through the opening of fractures and faults by the process of dissolution forming dolines, canyons, karstic bridges, sinks and springs with sharp top shapes, strong drainage density and slopes of 20–45% (IBGE, 1995). The recharging system comes from the Urucuia aquifer that feeds the rivers of the carbonate regions, locally represented by Vermelho e Buritis rivers. Typical features of karst, such as sinkholes, suffusion, and collapse types, are found on the surface (Ferreira and Uagoda, 2019) and also dry valleys, abandoned valleys, sinks, resurgence, and karrens where limestone are exposed (Motta, 2003).

The climate is tropical with seasonal characteristics, presenting a dry period (April to September) and a rainy one (October to March) with precipitation index of approximately 1260 mm.y $^{-1}$. The average annual temperature is 24 °C and the vegetation is typical of the Cerrado. Recent works (Nunes and Uagoda, Unpublished results) points out the main types of soils correspond to Quartz Neosols (43.1%) associated with plains, consisting basically of sand (>90%) with a mineralogical composition containing quartz and kaolinite; Chernossols (19.3%) in the middle slope mainly in carbonate areas having a hard and prismatic clay texture; and, Oxisols (13.3%) present in the plateaus. These later soils have a frank clay-sand texture, and identification was performed considering presence low activity clays (mainly kaolinite) and oxides (hematite and goethite). These soils types point out to weathering processes in humid and hot conditions in which the erosion is responsible for their removal and transportation under caves.

## 3. Tarimba cave

The Tarimba cave is an important cave in the Brazil scenario because of its extension and also because of the occurrence of endemic species such as the fish *Ituglanis Boticário* (Rizzato and Bichuette, 2014). The Tarimba cave is located at the boundary between the Bambuí Group and alluvial/colluvial deposits of Chapadão Formation, characterized by a covered karst. The exposure of limestone on surfaces that are often covered by soil, often originated from the sandstone's weathering, is located in a peripheral depression of a cuesta in regression (Hussain and Uagoda, 2021; SBE et al., 2014). The main Tarimba entrance (14°24′42.84″S and 46°10′29.63″W) is located in a large sinkhole indicating drainage capture to the cave's interior, as is showed in the topography (Fig. 2 A) and UAV image (Fig. 2 B). The area suffers from anthropic activities typically represented by agricultural practices as pasture (Fig. 2 E), which result in degradation and formation of bare soils (Fig. 2 C), increasing runoff and sediment production in the hilltops (Fig. 2D). This anthropogenic process can lead to karst desertification and a rise of the sediment amount entering the cave, which shows the correlation between sediment production and surface changes.

As a covered karst, near Tarimba cave, unconsolidated sediments of the Urucuia Group are observed on the top of the slope, lithic neosol on the medium slope and chernosols and limestone of the Lagoa do Jacaré Formation, Bambuí Group in the lower portions (Hussain et al., 2020). The patterns of surface runoff and aquifer recharge, connected to the different types of soil and rock and their characteristics, such as porosity and permeability (Hussain et al., 2020) are conditioning factors for removing and transport sediment under the cave.

The deposition of sediments at higher levels was controlled by the change of the hydraulic gradient of the mean Vermelho River, which consequently reflected in its tributary, Extrema River, which corresponds to the local base level. In the deep areas, a perennial flow is

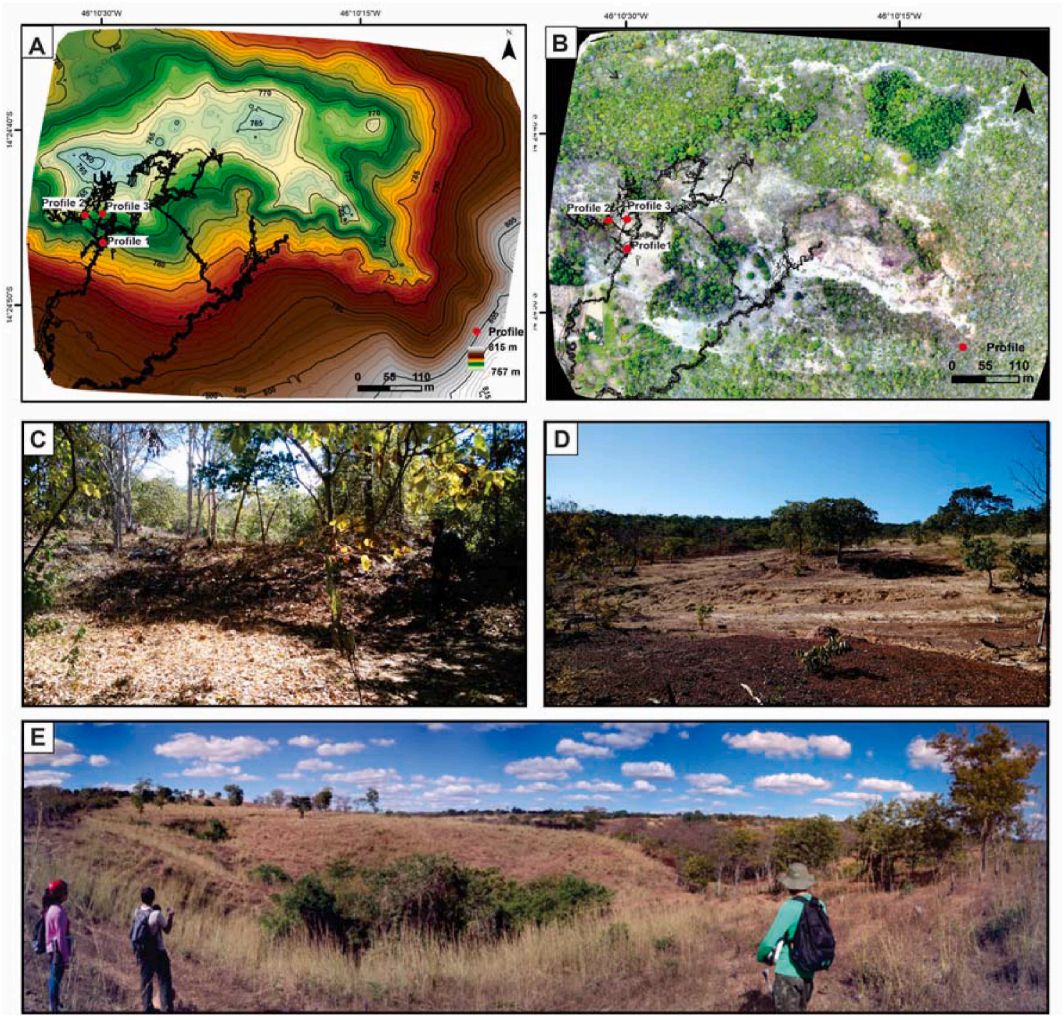


**Fig. 2.** Landscape surrounding Tarimba cave. A - Hypsometric map. B- High resolution image in which the whitish shades represent the unconsolidated sediments of the Urucuia Group sedimentary deposits at the top of the slopes. D - Main entrance of Tarimba cave. E – Soils with advanced degradation process in the cave adjacencies. F - Sinkhole in one of the entrances. Pictures: Dandara Caldeira, Renan Smith Penido Louzada and José Gustavo da Silva NuneS. (For interpretation of the references to color in this figure legend, the reader is referred to the Web version of this article.)

observed that, during the rainy periods, receives an essential amount of water and load from runoff. The underground interconnections, still unknown, are in the mapping phase, but the landscape suggest a connection between the Tarimba cave and the sink in the Extrema River.

Tarimba is Classified as a vadose cave on the upper galleries, dendritic with a tendency to rectilinearity of the conduits being an anastomosed at the entrances, what is attributed to the existence of several collectors and sedimentary concentration that cause the entanglement of the passages (Motta, 2003), as can be seen on the total topography of the cave (Fig. 3-A) and in the studied detail (Fig. 3 B). The cave presents a diversified development exhibiting an average vertical amplitude of 17 m in the highest part and decreases drastically up to 2 m in some paths sheltering countless fossil galleries (Motta, 2003). Currently, it does not receive visitation due to the narrow and deep pipelines that make tourism dangerous, especially during rainy periods.

There are large quantity and variety of speleothems with well-decorated halls. The cave horizontal floor is composed of compacted sediments, with lateral continuity (Fig. 3F) confirmed through the profiles studied in this article (Fig. C, D and E). The cave ceiling is rectilinear with evidence of sedimentary deposition on the sides and paleo floors, indicating more than one phase of sedimentation/erosion.

The Tarimba cave was chosen due to: 1) the importance of the cave hydro sedimentology system; 2) several contemporary studies are being carried out to manage the Vermelho River Rising Environmental Protection Area (APARNRV); 3) sedimentary deposits are accessible near the main entrance of the cave.

## 4. Method

The method applied in this study comprises the choice of one main deposit (Profile 1) (Fig. 3 C) and two others (Profiles 2 and 3) to allow the facies interpretation (Fig. 3-D and E). Those three profiles were chosen because they include extensive preserved sedimentary records, unlike other ones along the cave entrance. Furthermore, the path to the cave interior is difficult and dangerous due to its narrow configuration. The geometry on the chosen portion with plain floor and available deposits allows the survey work. This research consists of description and sampling based on accessibility, thickness, positioning in the cave, and the stratigraphic architecture of the deposit. The approach applied consists of several methodologies, combining grains size, roundness, facies analysis, geochemistry (IPC-OES), X-ray, and geochronology (Optically Stimulated Luminescence and Carbon 14), Fig. 4.

Profile 1 (P-1) shows the main deposit, which is located in the most distal portion of the cave entrance, with about 5 m of thickness and presenting a diverse sediment deposition compared with the other profiles, in which clast supported medium angle level truncated low

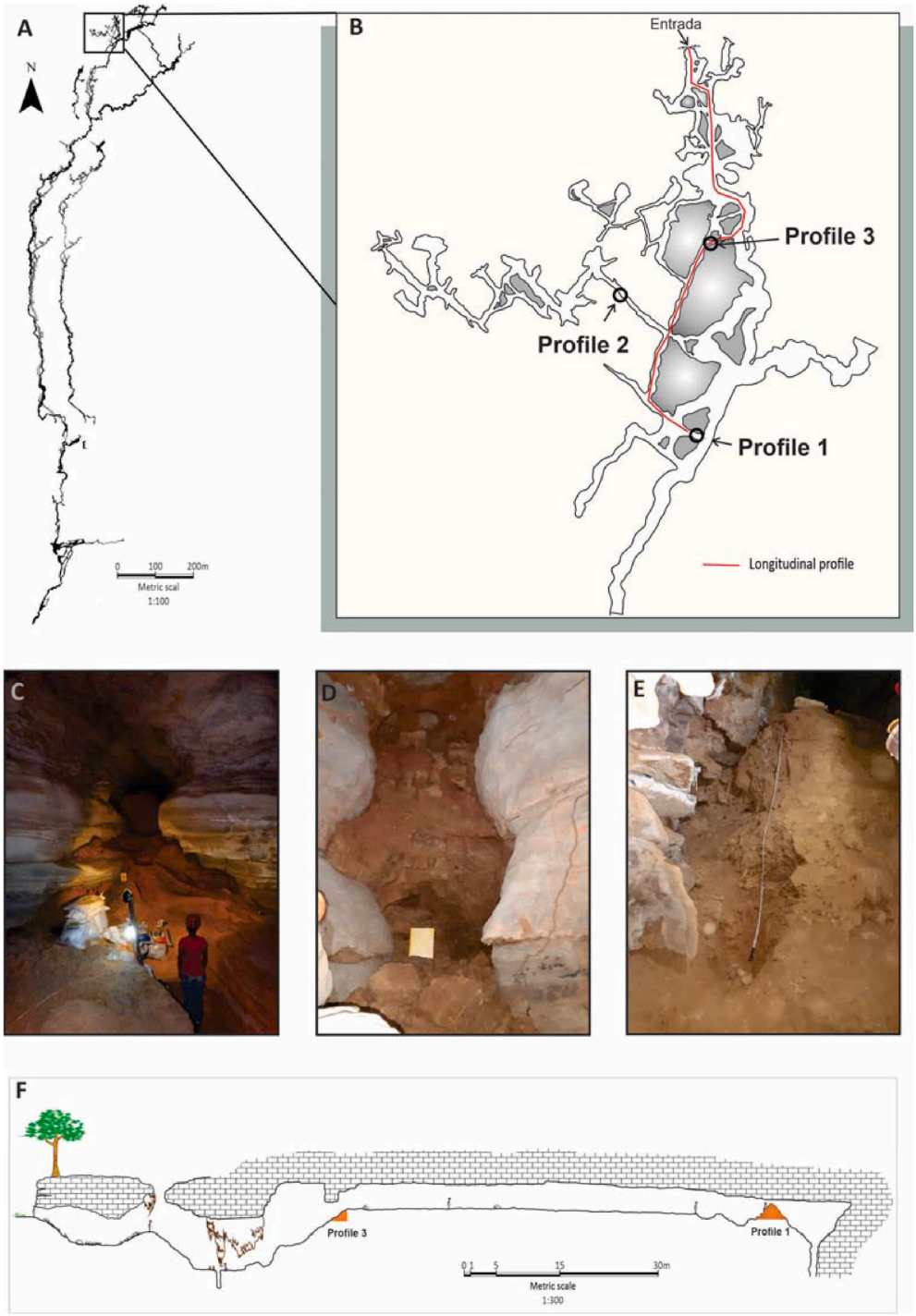


**Fig. 3.** A - Tarimba cave Map. B - Location of the sedimentary deposits studied: C - Profile 1, D - Profile 2 and E – Profile 3. F- Longitudinal profile from the entrance to Profile 1.

angle laminations of sand sediments. Due to specific characteristics such as unconsolidated sediments presence and stratigraphic architecture, the sampling was performed in two sections, central and lateral (columns A and B, respectively), Fig. 4. Such a situation implied a study in several levels (Units I to VII), interspersed by sample collection interruption in the sedimentary sequence.

Profile 2 (P-2) is located in the intermediate portion between the cave entrance and the most distal duct (P-1), in a 1.60 m thick conduit near the main one, where clay-sand sediments are distributed in bands, probably filling up to the roof. Profile 3 (P-3), about 1.90 m thick, is located next to the Tarimba entrance and, because it is at a lower level, constitute a ladder that gives access to other deposits in which sand-clay sediments are distributed in decametric bands having on the top a horizontal calcitic floor that serves as access to the other profiles.

### 4.1. Grain size analysis

The grain size analysis was performed at the Geochemistry and Water Laboratory – LAGEQ/University of Brasília, using samples collected at 10 cm intervals (n = 111 samples, where: 73 in P-1, 18 in P-2 and 20 in P-3),Fig. 4. The samples were air-dried, disaggregated, and sifted through the 2 mm and 1 mm sieve, and the larger fractions were

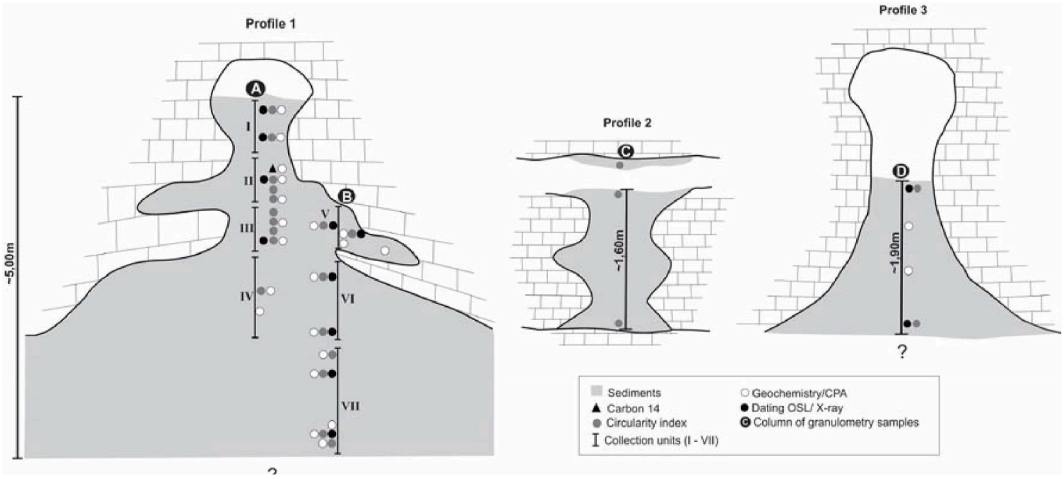


**Fig. 4.** Graphic synthesis showing the geometry of data collection in the profiles, with the collect level for each proxy. Location of Profiles 1, 2 and 3 in Tarimba cave can be seen in Fig. 3.

weighted. To eliminate organic matter from sediments smaller than 1 mm, Hydrogen Peroxide ($H_2O_2$) was used, followed by chemical (Sodium Pyrophosphate – $Na_4P_2O_7$) and physical (30 min in 50W ultrasound) dispersants. The remaining fractions were analyzed using the Bettersize ST Granulometer, using the LALLS – Low Angle Laser Light Scattering method, which is based on the fact that the diffraction angle is inversely proportional to the particle size.

A smaller number of samples (n = 23, where: 18 in P-1, 3 in P-2, and 2 in P-3) was selected, and its grain shape was determined by an automated analysis performed by the Bettersize S3 equipment in the ACIL & Weber Laboratory (São Paulo, Brazil), following an internal procedure (Fig. 4). Initially, the data were inserted, and a blank measurement was taken. Then, the samples were added directly to the analytical well with agitation of 1600 rpp and ultrasound (50W), posteriorly added to the chambers (0.5x and 10x) for a wider analytical range, and then the analysis was performed. Data were analyzed using the model system with the data treatment and grain size calculation software of the equipment (Bettersize Laser Particle Size Analysis System V8.0), based on the *ISO standards 13320-1(1999)* and *9276-1(1998)*. The main parameter to be obtained is the Circularity Index (CI), which indicates particle rounding (Equation (1)):

$$CI = \frac{4\pi x Area}{Perimeter^2} \quad (1)$$

### 4.2. Facies analysis

Facies analysis was performed based on lithological and sedimentary features, relative to the concept of sedimentary units defined by Anderton (1985) and the classification for caves proposed by White (2007). It was mainly observed features such as carbonate content, grain size and classification, and the presence of sedimentary structures. In order to determine correlations between the sedimentary environments, it was established an association of facies that consists of a cluster of spatially and genetically related facies (Martini, 2011). The delimitation of the facies allows understanding the sedimentation environment, concentrating on the origin of the sediments, and combined with geochronological methods, that corroborates the understanding of the evolution of the landscape (Hubbe et al., 2011).

### 4.3. Geochronology

Twelve samples were collected from the sandy units to be dated by Optically Stimulated Luminescence (OSL), with 10 samples from P-1 and 02 from P-3 profiles (Fig. 4). Opaque PVC pipes were inserted horizontally to retrieve sediment samples under dark conditions. Sediments from the edge of the tubes were discarded to avoid eventually light exposed sediments.

OSL dating was applied on quartz sediment grains isolated according to the procedures described by Aitken (1998): 1. Wet sieving to separate the 180 μm–250μm fraction; 2. Hydrogen peroxide ($H_2O_2$) treatment to eliminate organic matter; 3. Hydrochloric acid (HCl, 10%) treatment to eliminate carbonates; 4. Separation of light from heavy minerals in lithium metatungstate (LMT) solution with a density of 2.75 g/cm$^3$; 5. Separation of quartz from feldspar in an LMT solution with a density of 2.62 g/cm$^3$; 6. Hydrofluoric acid (HF, 38%) etching for 40 min to eliminate remaining feldspar grains and the outer layer of quartz grains dosed by alpha radiation; 7. Wet-sieving to eliminate etched grains finer than 180 μm. After these procedures, infrared (IR) stimulation was used to check for possible contamination by feldspar in quartz concentrates.

The luminescence measurements were performed on a Risø TL/OSL DA-20 reader from the Gamma Spectrometry and Luminescence Laboratory (LEGaL) of the Institute of Geosciences of the University of São Paulo (IGc-USP). The reader is equipped with blue LEDs (peak emission at 470 nm) and infrared LEDs (peak emission at 870 nm) for stimulation, beta irradiation source ($^{90}Sr/^{90}Y$) with a dose rate of 0.120 ± 0.004 Gy/s, and Hoya U-340 filters for light detection in the ultraviolet band. The equivalent dose (De) was estimated using the single-aliquot regenerative dose (SAR) protocol (Murray and Wintle, 2000) as described in Table 1. Dose recovery tests were performed to set up the measurements conditions for the dose range of the studied samples. Equivalent doses were calculated using the Central Age Model (CAM) (Galbraith et al., 1999). Only aliquots with recycling ratio within 0.9–1.1 range, recuperation

**Table 1**
OSL-SAR protocol used for equivalent dose estimation. Di: D1<D2<D3<D4; D5 = 0 Gy, D6 = D1; D7 = D6 (with IR stimulation before the OSL). Dose response curves were built using signals (Li/Ti) from D1 to D4. The signal of D5 was used to calculate recuperation. Recycling ratio was calculated through signals from D1 and D6. The relation between signals from D6 and D7 was used to appraise feldspar contamination.

| | Step |
|---|---|
| 1 | Dose (Di) |
| 2 | *Pre-heat* at 200 °C for 10s |
| 3 | Blue light stimulation at 125 °C for 40s ($L_i$) |
| 4 | Teste dose ($D_t$) |
| 5 | *Pre-heat* at 160 °C |
| 6 | Blue light stimulation at 125 °C for 40s ($T_i$) |
| 7 | *Blue bleach* at 280 °C for 40s |

less than 5% and negligible IR signal were used for equivalent dose calculations. The OSL signal was calculated, integrating the first 0.8 s of light emission and the last 10 s as background. Dose response curves were fitted using a single-saturating exponential function.

The radiation doses rates were estimated from $^{238}U$, $^{232}Th$ e $^{40}K$ concentrations determined by high-resolution gamma-ray spectrometry using a High Purity Germanium (HPGe) detector (energy resolution of 2.1 keV and relative efficiency of 55%) encased in an ultralow background shield. The samples were dried and packed in sealed plastic containers for storage during a minimum period of 28 days for radon requilibration before gamma ray spectrometry. Water saturation was determined from the ratio between water weight and dry sample weight. Radionuclide concentrations were converted into dose rates using conversion factors outlined by Guérin et al. (2011). Cosmic radiation contribution to the dose rate was calculated using longitude, latitude, altitude, and burial depth of each sample, according to the model proposed by Prescott and Stephan (1982).

One sample of organic matter in P-1 was dated using Accelerated Mass Spectrometry (AMS $^{14}C$) in the Beta Analytic – Testing Laboratory (Miami, Florida, United States), following internal procedures (Fig. 4). To calibrate the ages, the software BetaCal3.21: HPD and the method SHCAL13 were used. The "conventional radiocarbon age" was calculated using Libby's half-life (5568 years), and the results were credited by ISO/IEC-17025: 2005. Total fractionation effects were corrected from the radiocarbon conventional ages, and the calibration was performed using calibration databases from 2013.

### 4.4. Geochemical and mineralogical analysis

The analysis of the major elements ($SiO_2$, $Al_2O_3$, $Fe_2O_3$, CaO, MgO, $Na_2O$, $K_2O$, $TiO_2$, MnO, $P_2O_5$, and Loss on ignition - LOI) was performed on twenty-two samples (Fig. 4). The samples were air-dried, crushed, and homogenized in an agate mill and digested by fusion of lithium borate. The solutions obtained were analyzed by Inductively Coupled Plasma Optical Emission Spectrometer (ICP/OES), Agilent 5100 model, in the Geochemistry and Water Laboratory (LAGEQ) of the University of Brasília (Brazil). To compile the data, a Principal Component Analysis (PCA) was used, which is based on the relationship between the original variables using the PAST software.

Sediment's qualitative mineralogical analysis (total fraction) were performed on a selection of twelve samples using X-ray diffraction at the Diffractometry Laboratory of the University of Brasília. The diffractometer RIGAKU, ULTIMA IV model, equipped with copper tube and nickel filter under 35 kV and 15 mA current at a scanning speed of 2 θ/min in a scanning interval from 2° to 60°, velocity of 5°/min and step of 0.05°. The resulting diffractogram was analyzed and the identification of the minerals was performed with the aid of the program Jade XRD 9.0 (Materials Data), Windows-based, with database ICDD pdf-2 and pdf-4 (Power Diffraction File – PDF to PC – ICDD).

### 4.5. CIA (Chemical Index of Alteration)

The intensity of the chemical weathering can be evaluated by several proxies estimated from compositional indices (WIP, CIA, CIW, PIA, CIX, eg.). These proxies are widely used to infer paleoclimate conditions and more especially the weathering intensity. Therefore, the value of the index increases with the intensity of the weathering (Dinis et al., 2020).

Although it is probably the most used, the CIA (Chemical Index of Alteration) is not appropriate in establishing CaO bound to carbonate since the mobility of Ca and Mg is predominantly controlled by the behavior of calcite and dolomite (Buggle et al., 2011; Garzanti and Resentini, 2016). Thus, it was decided to apply the Chemical Proxy of Alteration (CPA) $Al_2O_3/(Al_2O_3 + Na_2O)$ x 100.

## 5. Results

### 5.1. Grain size analysis

The granulometric analysis yielded unconsolidated sand sediments, predominated by fine sand. Such sediments have continuous and sometimes extensive sand phases that are interspersed with finer sediments, mainly clay, indicating a change in hydraulic conditions of the deposition and/or variation in the source.

In Profile 1, the upper part of units I, VI, and VII converge to similar situations with deposition of essentially sandy sediments in horizontal layers (Figs. 5 and 6). Besides this pattern, lower central (Unit IV) and upper portions on the side of the profile (Unit V) stand out for the presence of silt-clay sediments and gravel. Also, units II and III present an irregular deposition with an adverse configuration related to the others, characterized by sandy levels with significant amounts of gravel.

From the base to the center of Profile 2, can be seen a change from greater amounts of sand to silt sediments (Fig. 7). The top, unlike the other sedimentary sequences, presents a prevalence of clay and silt with no sand, indicating an extremely slow flow. A sample from the ceiling reveals features like the lower strata and may indicate the resumption of a more intense flow that filed the conduit.

Grain size data of the Profile 3 showed a gradual decrease in silt quantity, in contrast with a gradual increase in the sand, and this trend is observed from the base to the middle of the profile (~1.0 m depth), Fig. 7. From the middle to the top, the levels are essentially sandy with only one inversion of values (~1.4 m). Such dynamics may indicate a progressive decrease in flow, followed by a considerable increase that culminates in a temporal gap with deposition of the paleofloor on the top.

Circularity index data are homogeneous in both profiles, and no dominant pattern was found. The values with a mean of 0.829 are close to good roundness, around 1, with few levels in the order of 0.7, both in Profile 1 (Fig. 8). Such characteristics can be attributed to the aqueous sedimentary transport, in which grain borders are smoothed, as well as due to abrasive processes (Campaña et al., 2016). However, the high degree of roundness also found in the sediments of the Urucuia Group (Iglesias and Uhlein, 2009) indicates that such characteristics originate from the source area and not necessarily from processes inside the cave.

### 5.2. Facies description

In the Tarimba cave, the sedimentary deposits were grouped into eight different facies represented by autochthonous and allochthonous sediments (Table 2 and Fig. 9- A,B,C,D). The Guano deposits (facies) represent phosphate accumulation and are the only sediments of autochthonous origin, corresponding to fecal material of animals. They occur as black sediments with whitish portions at the top of the section. In the allochthonous deposits, fine-grained sediments (silt and clay) are predominant, but they can contain up to 35% of sand and 15% of gravel (Fig. 9 – E). Following the classification of White (2007), the allochthonous sediments were separated into two main groups comprising four facies (Diamictiton, Channel, Backswamp, and Slackwater). Following the classification of White (2007), the allochthonous sediments were separated into two main groups comprising four facies (Diamicton, Channel, Backswamp, and Slackwater).

The Diamicton facies represents high density gravity flow and would results from extreme rainfall events and sediment flux in high gradient cave passages yielding in a massive and poorly sorted sedimentary deposit (White, 2007). In the Tarimba cave, they occur exclusively in the sides of Profile 1 and also in a configuration of lateral accretion and intercalated with the Channel facies (Fig. 9 – F, G). This facies is formed by poorly-sorted sediments represented by clast-supported massive gravel, with about 20–35% of gravel of varied roundness degree and sand-silt matrix composed of 34–55% of sand, 15–25% of silt, and less than 10% of clay.

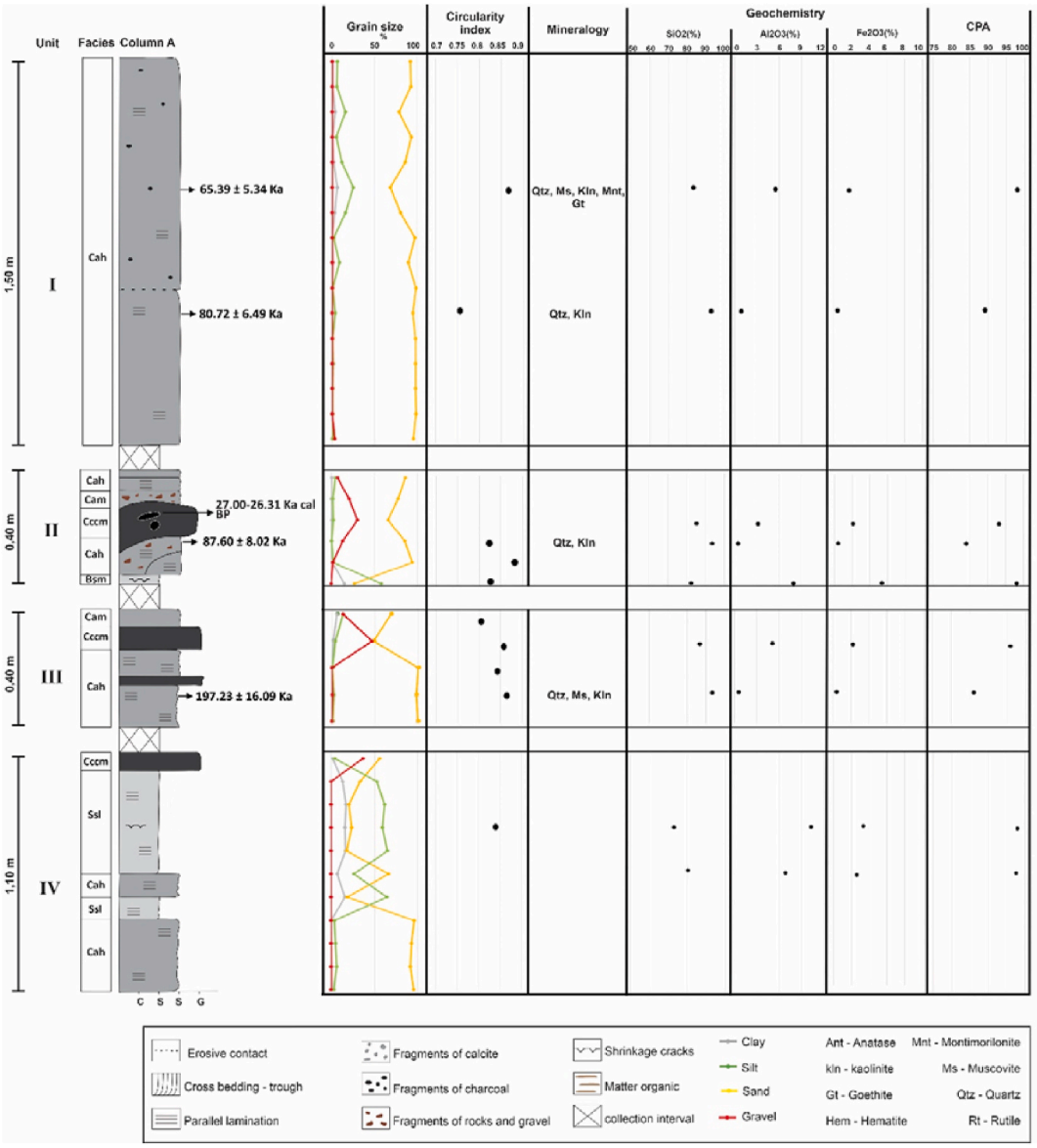


**Fig. 5.** Sedimentary facies, ages, textural and compositional data obtained in Column A of Profile 1. The location of the column is shown in Fig. 4.

The alluvial deposition is the main sedimentary process responsible for sediment deposition inside the cave. The alluvial deposits are represented by Channel, Backswamp, and Slackwater facies, ranging from clay to gravel. Fractures and cracks in the surroundings, are absent and the water transport is interpreted in association with the existence of an active watercourse with the surface at ~8 m below the location of the deposit, in addition to lamination and cross-stratification pointing to water-laid sediment transport.

The Channel facies occurs in all studied profiles and is the most common in Tarimba cave. Its deposits can be stratified, showing layers with similar thicknesses, different shades, well-defined contacts, and poor to moderately sorted sediments, which may also contain levels with organic matter besides fragments of charcoal and calcite crusts (Fig. 9). The Channel deposits comprise sandy channel facies and gravelly channel facies. The sandy facies have over 60% of very fine to coarse sand, with mean values above 90%. The gravelly facies are found in minor proportions and can reach up to 20% of gravel, with 35% of silt, and 7% of clay. The definition of these facies is essentially based on the observed sedimentary structures (Fig. 9- H, I, J, K).

The Channel facies with gravel, defined as clast-supported structureless gravel – Cccm, is similar to the Dccm facies due to the high amount of gravel (30–46%) (Fig. 9– G, H). However, it is differentiated by a matrix with 45–65% of sand and a low quantity of silt/clay (<5%). Another difference is that their sediments are moderately sorted, as opposed to those originated by flow debris and always occur associated with the sandy channel facies. Sometimes, it presents low cohesion, which would be characteristic of the minor amount of fine-grained sediments and lack of cementation.

The Backswamp facies is interpreted as suspended sediments transported by cave streams and fastly deposited by decantation in calm water settings (Campaña et al., 2017). It corresponds to Bsm facies with high content of very fine to fine silt that may reach more than 80% of the deposit, and above 50% of clay, with minor amount of gravel. Less than 30% of sand is found, although the average value is around 10% with a few levels above 20%. It is formed by ocher yellow, brown, and red sediments, often covered by a black coating pointing to oxidation. Sometimes, it is organized in the form of massive prismatic blocks with contraction cracks in some portions. It occurs predominantly in P-2 and P-3, usually associated with channel facies in an alternating deposition (Figs. 7 and 9- K).

The Slackwater facies is formed from the combined deposition of sediments by decantation and traction originating from flooding or

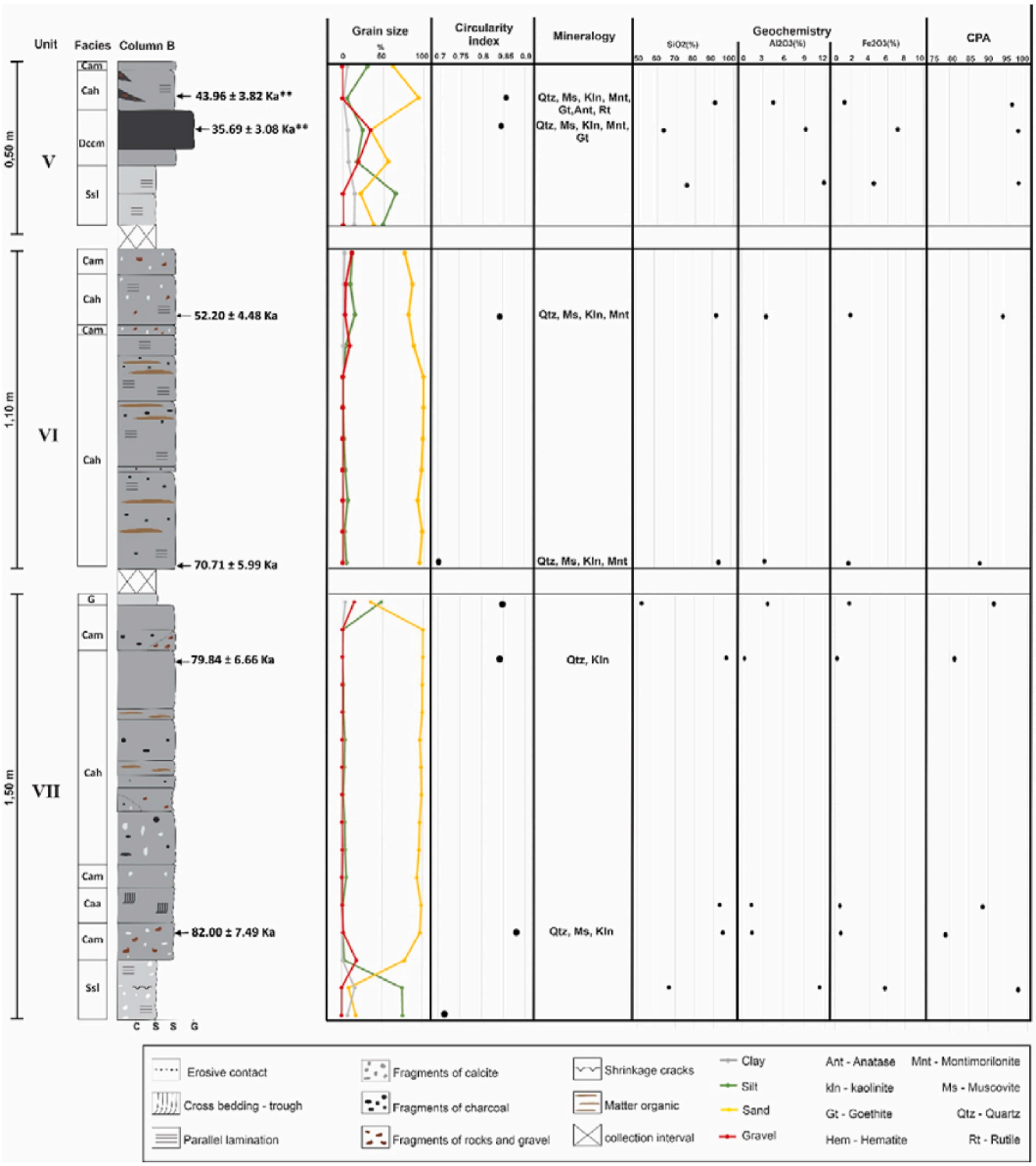


**Fig. 6.** Sedimentary facies, ages, textural and compositional data obtained in Column B of Profile 1. The location of the column is shown in Fig. 4.

pulsed flow (Ford and Williams, 2007; White, 2007), leading to the formation of heterolithic lamination. In the studied profiles, it corresponds to Ssl facies that resembles Bsm facies, but differs mainly for having laminations (Fig. 9– L). Sometimes, it presents contraction cracks, besides a smaller clay amount (maximum of 30%), and higher content of sand, with an average of 20% that may reach up to 37%. It shares the highest silt content (45–75%) and the lower amount of gravel. It occurs only in P-1, associated to the Diamicton or Channel facies as well as in the lower central portion of the cave (Unit IV).

### 5.3. Geochronology

The geochronological results are shown in Tables 3 and 4. In P-1, the obtained ages range from 50 to 90 Ka (Units I, II and VII, Figs. 5 and 6). In their upper portion, two dates differ from the rest: the OSL age of 197 Ka (Unit III) represents the bottom of the succession, but it must be analyzed with caution and associated with other proxies and observations since incomplete bleaching of quartz grains can occur in cave environments, leading to age overestimation (Jacobs et al., 2011; Rhodes, 2011; Constantin et al., 2014). However, all samples presented equivalent dose distributions with overdispersion ranging from 10 to 25% (Table 2). These overdispersion values suggest sediments well bleached prior to deposition and absence of significant post-depositional mixing or dose rate heterogeneities. Some samples (two samples at P-3, and two samples at P-1, Unit V) have OSL signals in saturation. For these samples, minimum ages were calculated considering the double of the characteristic dose ($2D_0$) from dose response curves as a minimum equivalent dose. The saturated samples have higher dose rates, which would explain the signal saturation. All non-saturated samples have ages in stratigraphical order, which supports the reliability of the OSL ages to interpret the depositional history within the cave. It is also highlighted that the relatively low dose rate of non-saturated samples allowed a relatively extended age limit.

The second outlier age occur in Unit II, where the $^{14}C$ age (27.00–26.31 Ka cal BP) is significantly younger than the OSL ages (ages older than 50 Ka). One of the interpretations for the younger radiocarbon age may be due to the absorption of modern $^{14}C$ from $HCO_3$ in the flowing groundwater, resulting in age underestimation (Ford and Williams, 2007). Water containing humic acids that may have infiltrated in the deposited sediments is another possibility leading to radiocarbon

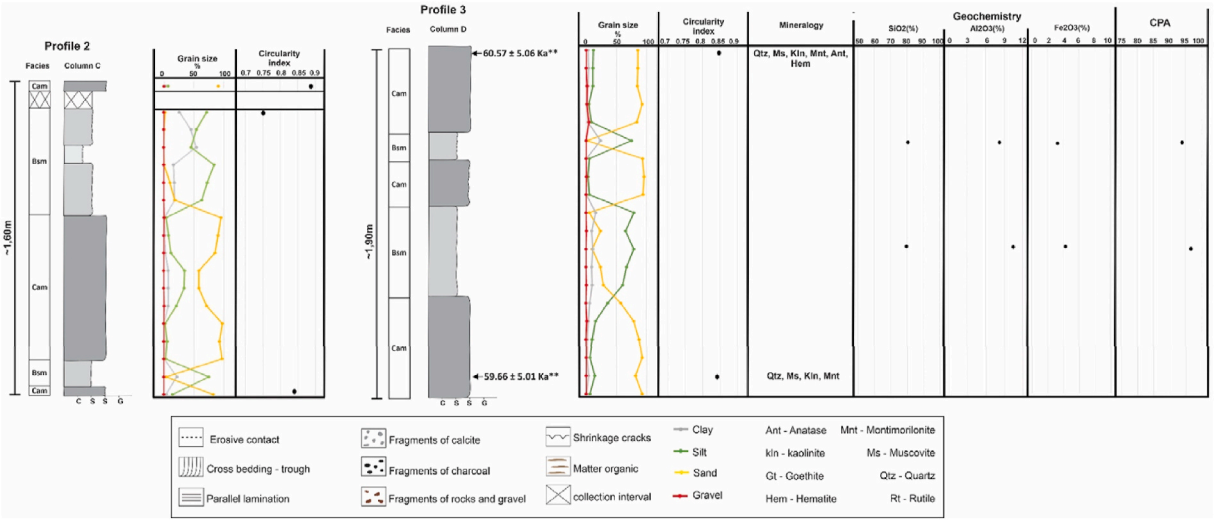


**Fig. 7.** Sedimentary facies, ages, textural and compositional data obtained in Profiles 2 and 3. The location of the column is shown in Fig. 4.

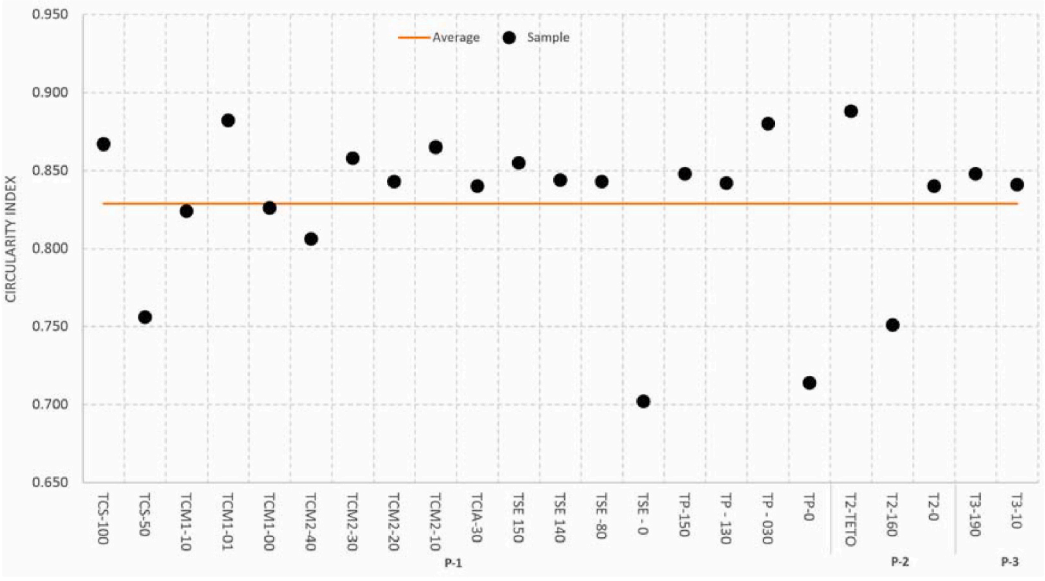


**Fig. 8.** Circularity Index results compared to the average Circularity Index (horizontal red line) from all samples. (For interpretation of the references to color in this figure legend, the reader is referred to the Web version of this article.)

**Table 2**
Sedimentary facies described in the studied deposits.

| Sediments Origin | Flow Type | Facies | Code | Description | Structure |
|---|---|---|---|---|---|
| Autochthonous | – | Guano | G | Guano | Structureless |
| Allocthonous | Debris flows | Conglomerate | Dccm | Clast-supported gravel | Structureless |
| | River flow | Channel | Caa | Fine to coarse sand that may contain gravel | Trough cross-bedding |
| | | | Cah | Fine to coarse sand that may contain gravel | Horizontal lamination |
| | | | Cam | Fine to coarse sand with occasional gravel | Structureless |
| | | | Cccm | Clast-supported gravel | Structureless |
| | | Backswamp | Bsm | Silt, clay and sand | Massive and contraction cracks |
| | | Slackwater | Ssl | Silt, clay and sand | Heterolithic lamination and contraction cracks |

age underestimation (Darrénougué et al., 2009). The other possible explanation would be the existence of long time lag between the entering of sediments in the cave (sunlight blocking and triggering of the OSL chronometer) and their final deposition in the studied profiles. However, the normal stratigraphic order of luminescence ages and equivalent dose distributions with low overdispersion, pointing to absence of post-depositional mixing, make this last explanation less plausible.

### 5.4. Chemical and mineralogical analysis

The results of chemical analysis can be seen in Figs. 5, 6 and 7 to for

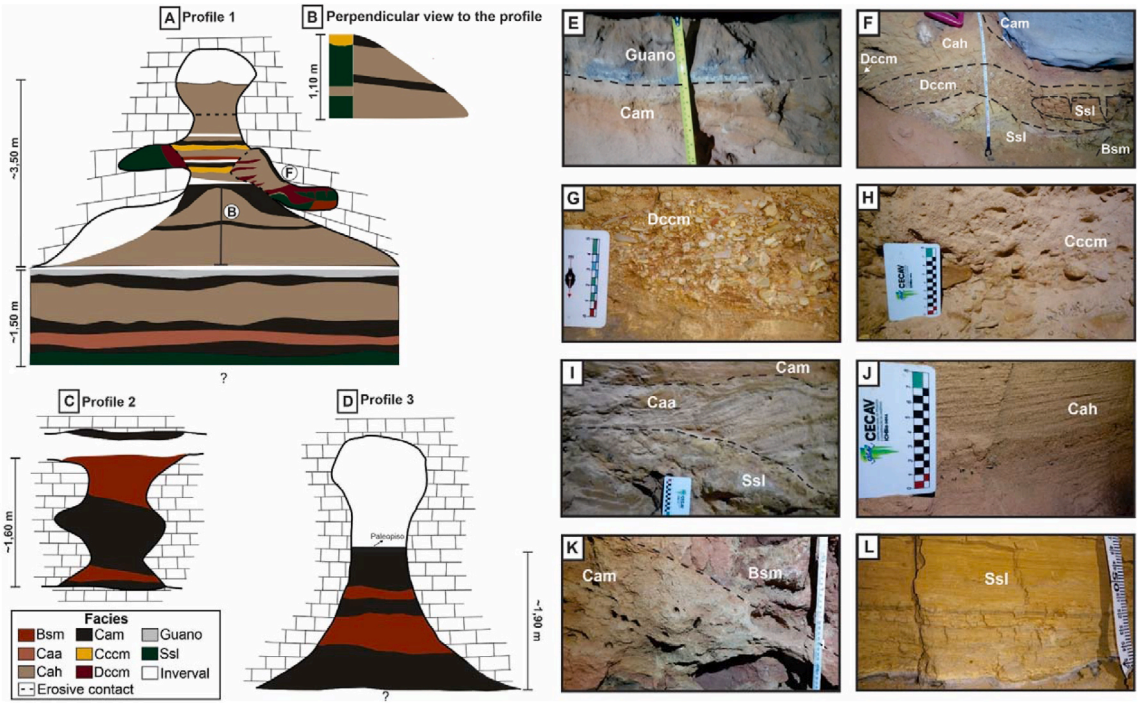


**Fig. 9.** Spatial distribution of sedimentary facies in profiles: A – Profile 1, B – Perpendicular view of the facies located on the base of Profile 1, C – Profile 2 and D – Profile 3. Pictures represent the facies found in the Tarimba cave (E, F, G, H, I, J, K, L).

the main data. The PCA of sediment data breaches into two principal components (Fig. 10), with 79% of the total variance. The PC1 (57%) shows high factor loadings for Al2O3, TiO2, FeO3, MgO, K2O, clay, and silt, and are grouped with Ssl and Bsm facies. Additionally. It also includes the Dccm facies that despite having high gravel content, also presents high levels of clay and silt.

The positive values of PC2 (22%) are related only to facies G, which may have values associated with animal feces (LOI and $P_2O_5$), and dissolution and precipitation processes on the surface (LOI and CaO). Finally, the negative values of PC1 and PC2, composed of $SiO_2$ and sand, delimitate the Channel facies (Cah, Cam, Caa, and Cccm).

The high CPA values from 70 to 98% demonstrate high weathering rates for these. Notoriously, there is a tendency for superficial layers to have higher values compared to intermediate and base layers that assume comparatively lower rates.

The qualitative mineralogical analysis is presented in Table 5, showing a similar composition between the facies that correlate with the homogeneous chemical composition. In general, there is a predominance of quartz and kaolinite in all facies analyzed, as well as muscovite and montmorillonite discontinuously along with the profile. Iron oxides and hydroxides such as hematite (Profile 3) and goethite (Profile 1 - Units I and V) occurred with lower recurrence, associated with the top of the sedimentary sequences. Minerals like anatase and rutile were exclusive to level of P-1 and P-3 (Figs. 5–7).

## 6. Discussion

### 6.1. Superficial environment and sedimentary deposition phases

The sediment deposition within the Tarimba cave is related to the superficial environmental dynamics. The sediments are originated from rocks of the Urucuia and Bambuí Groups (Figs. 1 and 2). This is supported by the compositional and grain size characteristics of the cave sediments, which present similarities with the soils mapped in the region. Three distinct compositional-textural groups of sediments are recognized: a) silt with high levels of $P_2O_5$ inside the cave; b) sandy sediments rich in $SiO_2$; c) fine sediments (clay and silt) containing a high percentage of $Al_2O_3$, $TiO_2$, $FeO_3$, MgO and $K_2O$. Such variations may indicate the existence of different sediment transport conditions and sources areas during the filling of the endokarst (Arriolabengoa et al., 2015). In the studied cave, the sediments constituting the described facies would be sourced from local areas. Hence, they allow to interpret changes in the local landscape over the last 200 Ka.

The oldest sedimentary records indicate a discontinuous deposition that occurred from the Middle Pleistocene to the Late Pleistocene, comprising an interval of around 145 Ka. The upper ducts filled with sandy-clayey sediments of metric thicknes were abandoned due to the reestablishment of the regional base level, generating the current cave configuration (SBE et al., 2014). The sedimentary facies, textural, compositional and geochronological data permitted to constrain the sedimentary evolution of the Tarimba. These data allowed to track the major depositional events and interpret possible landscape scenarios during the Late Quaternary.

Three phases of sediment deposition with established chronological intervals were found in Profile-1 (P-1,Fig. 11). Phase 1 comprises the oldest sediments of Profile 1 with age older than 197 Ka in contact with sediments of Unit V from 35 to 45 Ka (minimum age). However, the stratigraphic sequence bounded by erosive contacts could indicate older deposition. The lower and upper limits of the unit representing this phase are unknown. The lower limit was not reached during excavation and the upper is uncertain for not having any trace of accumulation in the ceiling of conduit. At least three depositional events can be identified in this phase (Fig. 11- a, b, c): the first (Phase 1a) represented by the SSL facies (Unit IV and V) indicates low energy water flow with oscillations characteristic of flooding facies followed by a period of removal and subarea exposure marked by contraction cracks (Phase 1b) (Figs. 5 and 6). This facies is truncated by an erosive phase and followed by a gravity flow depositional event (Phase 1c) with higher energy hydraulic conditions, capable of depositing massive gravel and fine sediments (Dccm facies) with progressive transition to Cah facies (Fig. 9 – F).

Phase 2 corresponds to Unity III and starts after an erosive event where the age with which part of the sediments of Phase 1 was removed from the central portion of the profile is unknown, leaving remaining material on the sides (Fig. 11– d, e). The lack of dating at the base makes

**Table 3**
Summary of OSL dating results.

| | Unit | Facies | Lab. cod. | Sample cod. | Depth (m) | Accepted/ measured aliquots | Overdispersion (%) | Water sat. | U (ppm) | Th (ppm) | K% | Total Dose rate (Gy/ Ka) | Equivalent dose (Gy) | OSL age (Ka) |
|---|---|---|---|---|---|---|---|---|---|---|---|---|---|---|
| **Profile 1** | I | Cah | L1228 | TCS-100 | 6.40 | 23/24 | 10.7 | 0.012 | 0.668 ± 0.042 | 3.292 ± 0.173 | 0.145 ± 0.011 | 0.610 ± 0.047 | 39.9 ± 1.0 | 65.39 ± 5.34 |
| | | Cah | L1227 | TCS-50 | 6.90 | 23/24 | 17.7 | 0.002 | 0.428 ± 0.024 | 0.857 ± 0.059 | 0.024 ± 0.004 | 0.260 ± 0.018 | 21.0 ± 0.8 | 80.72 ± 6.49 |
| | II | Cah | L1225 | TCM1-10 | 7.80 | 24/24 | 22.1 | 0.020 | 0.575 ± 0.036 | 1.821 ± 0.115 | 0.210 ± 0.012 | 0.539 ± 0.042 | 47.2 ± 2.2 | 87.60 ± 8.02 |
| | III | Cah | L1226 | TCM2-10 | 8.15 | 23/24 | 18.9 | 0.003 | 0.321 ± 0.020 | 0.695 ± 0.053 | 0.015 ± 0.003 | 0.207 ± 0.015 | 40.8 ± 1.7 | 197.23 ± 16.09 |
| | V | Dccm | L1223 | TSE-140 | 6.44 | 6/6 | – | 0.055 | 1.283 ± 0.056 | 11.263 ± 0.387 | 1.691 ± 0.072 | 2.740 ± 0.228 | 97.8 ± 2.2 | 35.69 ± 3.08[a] |
| | | Cah | L1224 | TSE-150 | 6.22 | 6/6 | – | 0.026 | 0.930 ± 0.042 | 7.344 ± 0.265 | 1.080 ± 0.046 | 1.872 ± 0.159 | 82.3 ± 1.6 | 43.96 ± 3.82[a] |
| | VI | Cah | L1221 | TSE-0 | 7.29 | 24/24 | 18 | 0.017 | 0.500 ± 0.027 | 1.551 ± 0.088 | 0.160 ± 0.009 | 0.457 ± 0.035 | 32.3 ± 1.2 | 70.71 ± 5.99 |
| | | Cah | L1222 | TSE-80 | 6.69 | 22/24 | 10.9 | 0.018 | 1.626 ± 0.072 | 2.741 ± 0.158 | 0.242 ± 0.015 | 0.889 ± 0.071 | 46.4 ± 1.4 | 52.20 ± 4.48 |
| | VII | Cam | L1220 | TP-30 | 7.20 | 24/24 | 26.2 | 0.011 | 0.268 ± 0.020 | 1.200 ± 0.072 | 0.124 ± 0.007 | 0.344 ± 0.026 | 28.2 ± 1.5 | 82.00 ± 7.49 |
| | | Cah | L1219 | TP-130 | 6.20 | 22/24 | 18.3 | 0.003 | 0.295 ± 0.021 | 0.573 ± 0.052 | 0.006 ± 0.004 | 0.194 ± 0.014 | 15.5 ± 0.7 | 79.84 ± 6.66 |
| **Profile 3** | – | Cam | L1360 | T3-190 | 6.00 | 17/34 | – | 0.010 | 0.910 ± 0.042 | 5.426 ± 0.207 | 0.695 ± 0.030 | 1.400 ± 0.116 | 84.8 ± 0.9 | 60.57 ± 5.06[a] |
| | – | Cam | L1361 | T3-10 | 7.80 | 10/10 | – | 0.030 | 1.277 ± 0.053 | 7.321 ± 0.256 | 0.923 ± 0.040 | 1.805 ± 0.150 | 107.7 ± 1.4 | 59.66 ± 5.01[a] |

[a] Samples with signal in saturation - minimum age from $2D_0$.

**Table 4**
$^{14}C$ dating.

| | Unit | Lab code | Sample code | Depth (m) | Method | Material | Age (Ka $^{14}C$ BP) | Calibrated age (Ka cal BP) |
|---|---|---|---|---|---|---|---|---|
| Profile 1 | II | Beta - 510831 | TCM1-20 | 7.7 | AMS | organic sediment | 22.39 ± 0.07 | 27.00–26.31 |

the beginning of this event uncertain. However, it is known that around 197 Ka, a high energy flow deposited the sandy facies, which includes layers with plane parallel laminations inclined at an angle compatible with erosion also observed in other overlapping strata. At the top of the phase, coarser sediments such as gravel (Cccm facies) are observed, indicating an increase in energy flow that gradually decreases, intermediate sandy facies, until reaching slower levels marked by the deposition of fine sediments on the top. The presence of contraction cracks at the top of this sequence (Bsm facies) may indicate a time gap capable of providing a sub-area exposure of sediments. Geochemistry, mineralogy, and circularity index data resemble the sediments of Phase 3, corroborating to nearby sources despite the time interval of more than 100 Ka.

Phase 3 occurs during the Upper Pleistocene, corresponding to the range of 87 to 52 Ka (Units I, II, VI, VII, Figs. 5 and 6) marked by successive flows resulting from the oscillation of the water column in which recent sediments are transported through the upper passage of the profile, above the Bsm facies (Phase 2 thermal). This sequence results on the sediments spreading in the profile ground overlapping layers of phases 1 and 2, allowing to found chrono correlated sequences both in the base and top of the profile. (Fig. 11– f/g).

This correlation is observed in geochemistry, mineralogy, and grain size from the erosion surface that allows identifying a Phase 3a that involves an interval between 87 and 80 Ka (Unit II and base of unit I, Unit VII) and a Phase 3b between 70 and 52 Ka (Top of Unit I and Unit VI). Both phases have sandy sediments in which there are variations between the Channel facies and the presence of sedimentary structures reflects the change of the hydraulic behavior, which depending on the intensity, may even present levels with gravel (Cccm facies). At the top of the successions, a slight change in granulometry can be seen, with a decrease in the percentage of sand and an increase in finer sediments between 65 and 52 Ka old, which indicates a decrease in flow intensity. Finally, the Guano facies were deposited on the profile access floor from the stabilization of hydraulic conditions.

Profiles 2 and 3, used in a complementary way, have a similar depositional architecture not identified in P-1. This feature suggests that these sediments were not reached in P-1 or that they were removed during periods of more intense flow. Dating performed in P-3 are of little help in this case, given the saturation of the sediment, implying in the calculation of minimum ages (59.66 ± 5.01 Ka and 60.57 ± 5.06 Ka), and requiring future analysis to clarify it. Although there is an absence of

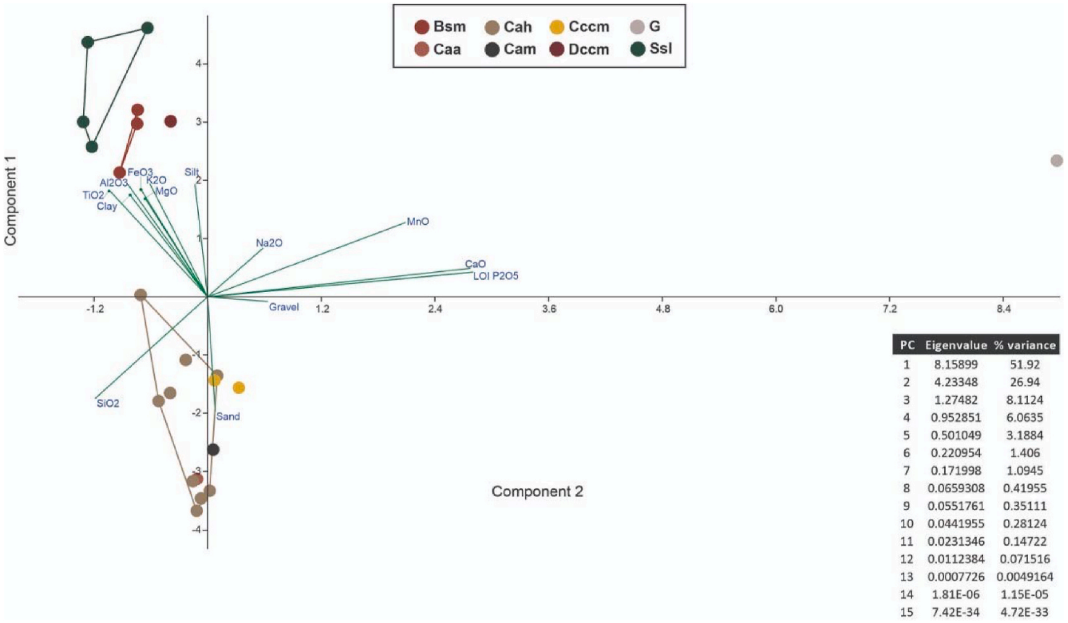


**Fig. 10.** Principal Component Analysis bi-plot for major elements in the sediments from Tarimba cave. The percentual of the component of each variance is in the right corner of the figure.

**Table 5**
Clay mineralogy result.

| | Unit | Facies | Sample | Quartz | Muscovite | Kaolinite | Montmorilonite | Goethite | Rutile | Anatase | Hematite |
|---|---|---|---|---|---|---|---|---|---|---|---|
| **Profile 1** | I | Cah | TCS-100 | X | X | X | X | X | | | |
| | | Cah | TCS-50 | X | | X | | | | | |
| | II | Cah | TCM1-10 | X | | X | | | | | |
| | III | Cah | TCM2-10 | X | X | X | | | | | |
| | V | Cah | TSE-150 | X | X | X | X | X | X | X | |
| | | Dccm | TSE-140 | X | X | X | X | X | | | |
| | VI | Cah | TSE-80 | X | X | X | X | | | | |
| | | Cah | TSE-0 | X | X | X | X | | | | |
| | VII | Cah | TP-130 | X | | X | | | | | |
| | | Cam | TP-30 | X | X | X | | | | | |
| **Profile 3** | – | Cam | T3-190 | X | X | X | X | | | X | X |
| | – | Cam | T3-10 | X | X | X | X | | | | |

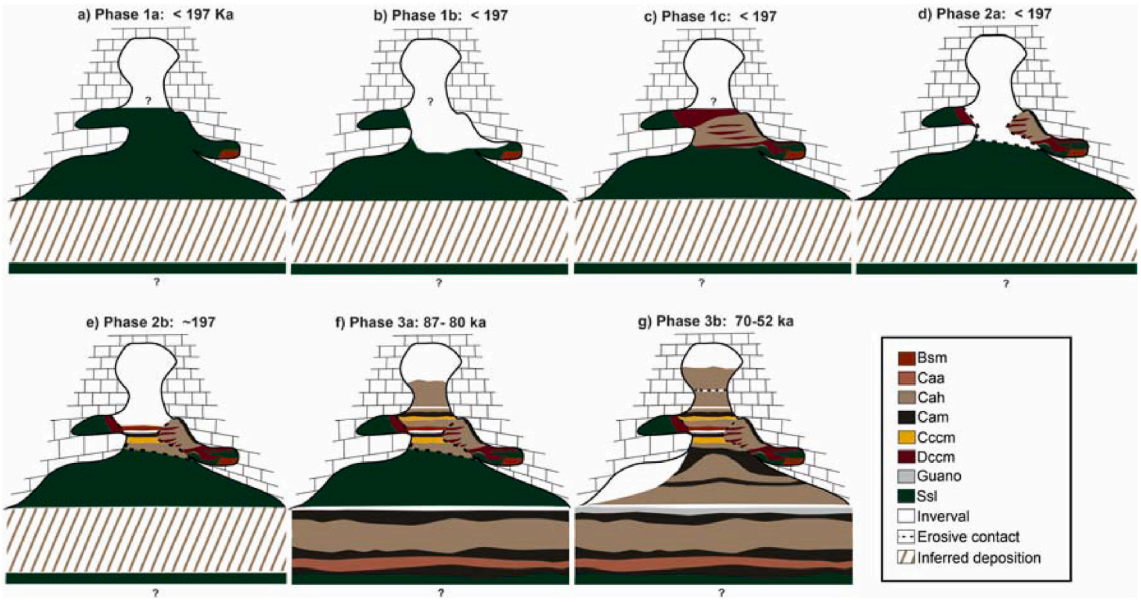


**Fig. 11.** Sedimentary deposition evolution in Profile 1.

geochronological data, the association between facies allows us to infer that profiles 2 and 3 are contemporary because at least three phases can be identified (Fig. 12): Phase A - resulting from alternating hydraulic flows corresponding to the filling of the ducts by Backswamp and Channel facies; Phase B – sediment removal preserving the studied sequences and material on the cave walls, exposing the profiles used in the study; and Phase C formation of the paleofloor in P-3 after stabilization of the sedimentation, which demonstrates the existence of a relatively humid period.

### 6.2. *Surface landscape erosion, climate change and cave sediment deposition*

The clastic deposits preserved in the Tarimba cave are derived from surface erosion, being product of the landscape evolution. The chronology of cave sedimentary deposits makes possible to constrain erosion and depositional events associated with the evolution of the relief over time, allowing the establishment of connections with environmental changes during the Quaternary. Studies with clastic sediments in the Brazilian caves have shown that the processes of erosion and deposition may be related to paleoclimatic variability. In dry climate settings, the entry of sediments in caves is controlled by episodic rainfall once that the absence of dense vegetation would increase soil erosion and sediment supply while in wet setting, the presence of a denser vegetation cover reduces erosive processes and sediment supply (Auler et al., 2002, 2009; Jaqueto et al., 2016; Haddad-Martim et al., 2017; Novello et al., 2019). However, this dynamics also depends of the fluvial processes and sediments temporary stored in river valleys (Herman et al., 2012; Laureano, 2014).

The absence of specific paleoclimatic records in the Tarimba region difficults the comparison between erosion-depositional phases and rainfall variations during the Late Quaternary. Then, we used weathering indexes (CPA) to deduce the erosion and deposition sedimentary dynamics of the landscape suppling sediment to the Tarimba cave. Furthermore, climatic conditions in the last 200 Ka were inferred by comparing our geochronological data with paleoclimatic records from speleothems of the Lapa Grande Cave, which represents climate conditions of Central Brazil (Stríkis, 2015). The chemical weathering indexes reflect the intensity of the climate action on the relief according to the exposure time, which will vary depending on the weathering material (Dinis et al., 2020). Although there is no consensus on the interpretation of such indexes, the use of CPA proved to be a reliable indicator of Quaternary climatic variability from sedimentary records inside the Mohui cave in China (Cheng et al., 2020).

The CPA index was calculated using data from Profile 1, excluding the deposits where we obtained only minimum OSL ages. The results show high weathering rates (79.22–98.58%) in which the highest rates are correlated with warmer and wetter conditions (Dinis et al., 2020). However, even in this scenario of high weathering rates, it is possible to infer three climatic situations that may have influenced the erosion dynamics. The first situation is represented by the lower CPA index, compared to the others (86.03%), which corresponds to the oldest depositional phase (Fig. 5) Such age can be correlated with the Marine Isotope Stage (MIS) 7 period (Unit III, Fig. 13).

The interval in which the CPA reaches lower values between 79.22 and 89.17% is represented by intermediate sediment layers with ages between 87 and 70 Ka, which are predominantly correlated with the MIS 5 (130-75 Ka), (Unit I, II, VI and VII, Fig. 13). Isotopic analyses of δ18O in speleothems from the Lapa Grande cave in the central-eastern region of Brazil showed that during the last glacial and Holocene period (60–85 Ka), the climate was predominantly drier with relatively low rainfall compared to the southernmost regions of Brazil (Stríkis, 2015).

In the last phase of sediment deposition (65-52 Ka), the weathering rate is higher (93.90–98.08%), suggesting wetter climate during the MIS 3 and MIS 4 (Unit I and VI,Fig. 13). Data on climatic conditions corresponding to the end of the MIS 3 period are absent. However, among the gaps identified throughout MIS 3 (between ~ 60 and ~27 Ka), the period between 49 and 40 Ka suggests the shift to a drier phase. It was also attributed to this period temperatures variations relate to stadial (cold) and interstadial (warm) phases (Stríkis, 2015).

Our survey shows that high weathering rates recorded by sediments preserved in the Tarimba cave indicate the predominance of warm and humid climates in the region during the last 200 Ka. However, according to the isotopic data from the Lapa Grande cave, the region was drier and with sporadic rainfall events. It must be highlighted that the clastic deposits can record only the major rainfall episodes while speleothems record average climatic conditions. Also, the sediment composition can represent long term weathering conditions for soil production, which can differ from the conditions prevailing during the phases of soil erosion and sediment transport to the cave. Thus, the deposition of clastic sediments inside the Tarimba cave occurred during drier periods, as showed by paleoclimate studies in central Brazil. As pointed out by Auler et al. (2009), past drier periods reduced the vegetation cover and exposed soil to erosion, increasing sedimentation rates during episodic rains. Considering the local character of the study setting, further studies will be necessary in order to test this explanation about how climate variations control the sedimentation in Brazilian cave systems.

## 7. Final considerations

The deposition of clastic sediments in caves is associated with the climate dynamics of the surrounding environment. In the case of Tarimba cave, the geomorphological processes active in the retreat of the relief provides the sediments of the Urucuia (sandy) and Bambuí (silt-clay) groups that are transported and deposited inside the cave. The establishment of new base levels by regional rivers is responsible for the

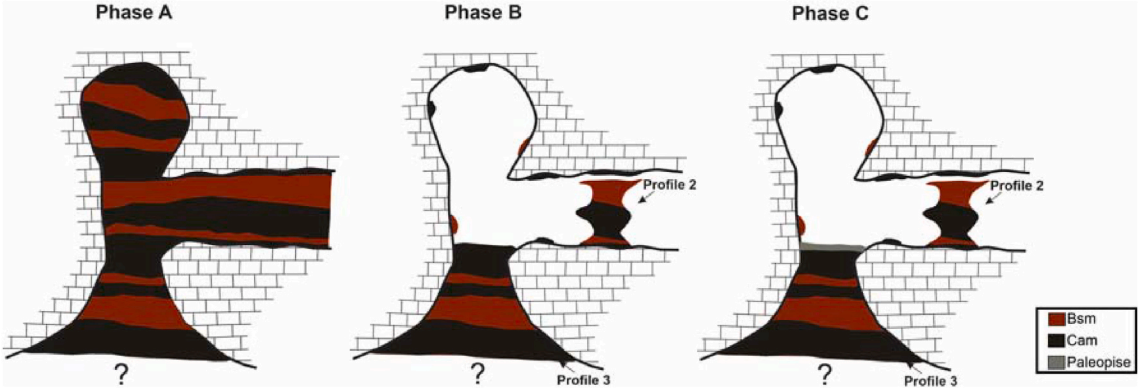


**Fig. 12.** Schematic section for depositional events that occurred in Profiles 2 and 3. **Use color for printed pictures.** (For interpretation of the references to color in this figure legend, the reader is referred to the Web version of this article.)

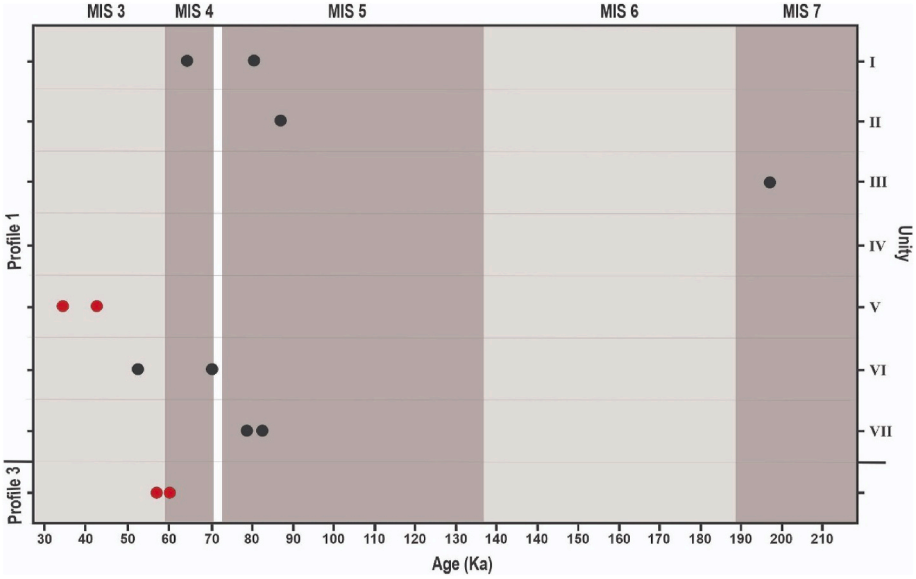


**Fig. 13.** OSL ages obtained from Profile 1, with the corresponding Isotopic Marine Stages (MIS). Black dots represent absolute ages, while red ones represent minimum ages. (For interpretation of the references to color in this figure legend, the reader is referred to the Web version of this article.)

abandonment of galleries crammed with sediments in the upper levels, allowing the establishment of three major sedimentary deposition phases in Profile 1 and two in Profiles 2 and 3. In the last 200 Ka, the depositional architecture as well as the sedimentary facies analysis allowed the interpretation of flow conditions of sediment deposition, which are represented by eight facies corresponding to the features currently found in the cave.

The results found three depositional phases in the studied profiles. The first one is relative to the oldest sediments, prior to 200 Ka, whose configuration indicates alternation of water flow energy transporting and forming a clast supported level. Contraction cracks indicate at least one period of sub-aerial exposure with an interruption in the deposition. The second phase begins after an erosive event and has at last one confirmed age of 197 Ka. Sandy sediments predominate, corresponding to the channel facies with oscillations in the energy and grain size gradation. The third phase is formed by channel facies as the second one, which comprises the interval between 87 and 52 Ka, subdivided into 87-80 Ka and 70-52 Ka, with alternation in the arrangement of sandy and silty facies that indicate an oscillation in the intensity of the hydraulic flow. The last phase establishing the current configuration visualized in the cave. The extensive amount of methodologies used offers important information for the development of future studies with a paleoenvironmental perspective in the Brazilian cave deposits.

## Financing

This work is part of the project “Susceptibilidade e Hidrogeomorfologia Cárstica da APA Nascente do Rio Vermelho/GO” funded by CECAV/ICMBIO, process n.02667.000110/2017–10.

## Declaration of competing interest

The authors declare that they have no known competing financial interests or personal relationships that could have appeared to influence the work reported in this paper.

## References

Aitken, M.J., 1998. An Introduction to Optical Dating. Oxford University Press, New York.

Anderton, R., 1985. Clastic facies models and facies analysis. Geol. Soc. Lond. Spec. Publ. 18, 31–47. https://doi.org/10.1144/GSL.SP.1985.018.01.03.

Araujo, V.A. de, Moreton, L.C., 2008. Unidades Litoestratigráficas. In: Geologia Do Estado de Goiás e Distrito Federal, pp. 43–113. Goiânia.

Arriolabengoa, M., Iriarte, E., Aranburu, A., Arrizabalaga, A., 2015. Provenance study of endokarst fi ne sediments through mineralogical and geochemical data (Lezetxiki II cave , northern Iberia). Q. Int. J. 364, 231–243. https://doi.org/10.1016/j.quaint.2014.09.072.

Auler, A.S., Smart, P., Tarling, D.H., Farrant, A.R., 2002. Fluvial incision rates derived from magnetotratigraphy.pdf. Zeitschrift für Geomorphologie 46, 391–403.

Auler, A.S., Piló, L.B., Smart, P.L., Wang, X., Hoffmann, D., Richards, D.A., Edwards, R.L., Neves, W.A., Cheng, H., 2006. U-series dating and taphonomy of Quaternary vertebrates from Brazilian caves. Palaeogeogr. Palaeoclimatol. Palaeoecol. 240, 508–522. https://doi.org/10.1016/j.palaeo.2006.03.002.

Auler, A.S., Smart, P.L., Wang, X., Piló, L.B., Edwards, R.L., Cheng, H., 2009. Cyclic sedimentation in Brazilian caves: mechanisms and palaeoenvironmental significance. Geomorphology 106, 142–153. https://doi.org/10.1016/j.geomorph.2008.09.020.

Ballesteros, D., Giralt, S., García-Sansegundo, J., Jiménez-Sánchez, M., 2019. Quaternary regional evolution based on karst cave geomorphology in Picos de Europa (Atlantic Margin of the Iberian Peninsula). Geomorphology 336, 133–151. https://doi.org/10.1016/j.geomorph.2019.04.002.

Buggle, B., Glaser, B., Hambach, U., Gerasimenko, N., Marković, S., 2011. An evaluation of geochemical weathering indices in loess-paleosol studies. Quat. Int. 240, 12–21. https://doi.org/10.1016/j.quaint.2010.07.019.

Campaña, I., Benito-Calvo, A., Pérez-González, A., Bermúdez de Castro, J.M., Carbonell, E., 2016. Assessing automated image analysis of sand grain shape to identify sedimentary facies, Gran Dolina archaeological site (Burgos, Spain). Sediment. Geol. 346, 72–83. https://doi.org/10.1016/j.sedgeo.2016.09.010.

Campaña, I., Benito-Calvo, A., Pérez-González, A., Ortega, A.I., Bermúdez de Castro, J. M., Carbonell, E., 2017. Pleistocene sedimentary facies of the gran Dolina archaeo-paleoanthropological site (Sierra de Atapuerca, Burgos, Spain). Quat. Int. 433, 68–84. https://doi.org/10.1016/j.quaint.2015.04.023.

Campos, J.E.G., Dardenne, M.A., 1997. Estratigrafia E Sedimentação Da Bacia Sanfranciscana: Uma Revisão. Rev. Bras. Geociencias 27, 269–282. https://doi.org/10.25249/0375-7536.1997269282.

Cheng, L., Bae, C.J., Hong, H., Huang, S., Wang, W., Yin, K., Wang, C., 2020. Environmental fluctuation impacted the evolution of Early Pleistocene non-human primates: biomarker and geochemical evidence from Mohui Cave (Bubing, Guangxi, southern China). Quat. Int. 563, 64–77. https://doi.org/10.1016/j.quaint.2020.02.035.

Cherem, L.F.S., Varajão, C.A.C., 2014. O papel da lito-ESTRUTURA do carste NA morfodinâmica cenozóica da serra geral de goiás (GO/TO/BA): aproximaÇÕES INICIAIS. Geonorte 10, 180–184.

Constantin, S., Robu, M., Munteanu, C.M., Petculescu, A., Vlaicu, M., Mirea, I., Kenesz, M., Drăguşin, V., Hoffmann, D., Anechitei, V., Timar-Gabor, A., Roban, R.D., Panaiotu, C.G., 2014. Reconstructing the evolution of cave systems as a key to understanding the taphonomy of fossil accumulations: the case ofUrşilor Cave (Western Carpathians, Romania). Quat. Int. 339 (340), 25–40. https://doi.org/10.1016/j.quaint.2013.10.012.

Cruz, A.B. da, 2012. Detalhamento da geologia das unidades carbonáticas do Grupo Bambuí na região de Alvorada do Norte. Goiás. Universidade de Brasilia.

Dardenne, M.A., 1981. Anais do Simpósio sobre o Cratón do São Francisco e suas faixas marginais. Os Grupos Paranoá e Bambuí Na Faixa Dobrada Brasília, pp. 140–157. Salvador.

Dardenne, M.A., Magalhaes, L.F., Soares, L.A., 1978. XXX Congresso Brasileiro de Geologia. Geologia Do Grupo Bambuí No Vale Do Rio Paranã (Goiás), Recife, pp. 611–621.
Darrénougué, N., Deckker, P. De, Fitzsimmons, K.E., Norman, M.D., Reed, L., Kaars, S. van der, Fallon, S., 2009. A late Pleistocene record of aeolian sedimentation in Blanche cave, Naracoorte, south Australia. Quat. Sci. Rev. 28, 2600–2615. https://doi.org/10.1016/j.quascirev.2009.05.021.
Dinis, P.A., Garzanti, E., Hahn, A., Vermeesch, P., Cabral-Pinto, M., 2020. Weathering indices as climate proxies. A step forward based on Congo and SW African river muds. Earth Sci. Rev. 201, 103039. https://doi.org/10.1016/j.earscirev.2019.103039.
Farrant, A.R., Smart, P.L., 2011. Role of sediment in speleogenesis; sedimentation and paragenesis. Geomorphology 134, 79–93. https://doi.org/10.1016/j.geomorph.2011.06.006.
Faure, M., Guérin, C., Parenti, F., 1999. Découverte d 'une mégafaune holocène do Serrote do Artur (aire archéologique de Sao Raimundo Nonato, Piauí, Brésil). C. R. Acad. Sci. Paris 443–448.
Ferreira, C.F., Uagoda, R.E.S., 2019. O uso de veículo aéreo não tripulado - VANT para construção de modelos digitais de terreno – MDT e identificação de dolinas na área da gruna da Tarimba-GO. ANAIS Do 35º Congresso Brasileiro de Espeleologia. Bonito/MS, pp. 52–62.
Fontugne, M., 2013. New radiocarbon ages of Luzia woman, Lapa Vermelha IV site, Lagoa Santa, Minas Gerais, Brazil. Radiocarbon 55, 1187–1190. https://doi.org/10.2458/azu_js_rc.55.16253.
Ford, D., Williams, P., 2007. Karst Hydrogeology and Geomorphology, Karst Hydrogeology and Geomorphology. Wiley, Chichester. https://doi.org/10.1002/9781118684986.
Galbraith, R.F., Roberts, R.G., Laslett, G.M., Yoshida, H., Olley, J.M., 1999. Optical dating of single and multiple grains of quartz from Jinmium rock shelter, northern Australia: Part I, experimental design and statistical models. Archaeometry 41, 339–364. https://doi.org/10.1111/j.1475-4754.1999.tb00987.x.
Garzanti, E., Resentini, A., 2016. Provenance control on chemical indices of weathering (Taiwan river sands). Sediment. Geol. 336, 81–95. https://doi.org/10.1016/j.sedgeo.2015.06.013.
Gaspar, M.T.P., Campos, J.E.G., 2007. O Sistema Aqüífero Urucuia. Rev. Bras. Geociencias 37, 216–226. https://doi.org/10.25249/0375-7536.200737s4216226.
Gillieson, D., 1996. Caves: Processes, Development and Management, 1º. Blackwell, Massachusetts. https://doi.org/10.1002/9781444313680.
Guérin, G., Mercier, N., Adamiec, G., 2011. Dose-rate Conversion Factors: Update Dose-Rate Conversion Factors: Update.
Haddad-Martim, P.M., Hubbe, A., Giannini, P.C.F., Auler, A.S., Piló, L.B., Hubbe, M., Mayer, E., Wang, X., Cheng, H., Edwards, R.L., Neves, W.A., 2017. Quaternary depositional facies in cave entrances and their relation to landscape evolution: the example of Cuvieri Cave, eastern Brazil. Catena 157, 372–387. https://doi.org/10.1016/j.catena.2017.05.029.
Herman, E.K., Toran, L., White, W.B., 2012. Clastic sediment transport and storage in fluviokarst aquifers: an essential component of karst hydrogeology. Carbonates Evaporites 27, 211–241. https://doi.org/10.1007/s13146-012-0112-7.
Hubbe, A., Haddad-Martim, P.M., Hubbe, M., Mayer, E.L., Strauss, A., Auler, A.S., Piló, L. B., Neves, W.A., 2011. Identification and importance of critical depositional gaps in pitfall cave environments: the fossiliferous deposit of Cuvieri Cave, eastern Brazil. Palaeogeogr. Palaeoclimatol. Palaeoecol. 312, 66–78. https://doi.org/10.1016/j.palaeo.2011.09.010.
Hussain, Y., Uagoda, R., 2021. GIS-based relief compartment mapping of fluvio-karst landscape in central Brazilian highlands. International Journal of Economic and Environmental Geology. https://doi.org/10.1002/essoar.10503441.2.
Hussain, Y., Uagoda, R., Borges, W., Nunes, J., Hamza, O., Condori, C., Aslam, K., Dou, J., Cardenas-Soto, M., 2020. The potential use of geophysical methods to identify cavities, sinkholes and pathways for water infiltration: a case study from Mambaí, Brazil. Water 12, 1–19. https://doi.org/10.3390/w12082289.
IBGE, 1995. Zoneamento Geoambiental e Agroecológico - Goiás/região nordeste, IBGE, Divi. Rio de Janeiro.
ICMBio/CECAV, 2017. RELATÓRIO DE VISTORIA TÉCNICA EM CAVERNAS E SUAS ÁREAS DE INFLUÊNCIA NA ÁREA DE PROTEÇÃO AMBIENTAL DAS NASCENTES DO RIO VERMELHO.
ICMBio/CECAV, 2020. Relatório Estatístico - Cavidades por UF. Brasilia.
Iglesias, M., Uhlein, A., 2009. Estratigrafia do Grupo Bambuí e coberturas fanerozóicas no vale do rio São Francisco, norte de Minas Gerais. Rev. Bras. Geociencias 39, 256–266. https://doi.org/10.25249/0375-7536.2009392256266.
Jacobs, Z., Meyer, M.C., Roberts, R.G., Aldeias, V., Dibble, H., Hajraoui, M.A. El, 2011. Single-grain OSL dating at La Grotte des Contrebandiers ("Smugglers" Cave'), Morocco: improved age constraints for the Middle Paleolithic levels. J. Archaeol. Sci. 38, 3631–3643. https://doi.org/10.1016/j.jas.2011.08.033.
Jaqueto, P., Trindade, R.I.F., Hartmann, G.A., Novello, V.F., Cruz, F.W., Karmann, I., Strauss, B.E., Feinberg, J.M., 2016. Linking speleothem and soil magnetism in the Pau d'Alho cave (central South America). J. Geophys. Res.: Solid Earth 121, 7024–7039. https://doi.org/10.1002/2016JB013541.Received.
Kinoshita, A., Skinner, A.R., Guidon, N., Ignacio, E., Felice, G.D., Buco, C. de A., Tatumi, S., Yee, M., Figueiredo, A.M.G., Baffa, O., 2014. Dating human occupation at Toca do Serrote das Moendas, São Raimundo Nonato, Piauí-Brasil by electron spin resonance and optically stimulated luminescence. J. Hum. Evol. 77, 187–195. https://doi.org/10.1016/j.jhevol.2014.09.006.
Laureano, F.V., 2014. Idades de Soterramento 26al/10 Be em grão de quartzo e o assoreamento de sistema de Cavernas Na Região Iraquara (Ba): 2 Milhões de anos de registro sedimentar Quaternário. Universidade de São Paulo, São Paulo.
Laureano, F.V., Karmann, I., Granger, D.E., Auler, A.S., Almeida, R.P., Cruz, F.W., Strícks, N.M., Novello, V.F., 2016. Two million years of river and cave aggradation in NE Brazil: implications for speleogenesis and landscape evolution. Geomorphology 273, 63–77. https://doi.org/10.1016/j.geomorph.2016.08.009.
Martini, I., 2011. Cave clastic sediments and implications for speleogenesis: new insights from the Mugnano cave (Montagnola Senese, northern Apennines, Italy). Geomorphology 134, 452–460. https://doi.org/10.1016/j.geomorph.2011.07.024.
McAdams, C., Morley, M.W., Fu, X., Kandyba, A.V., Derevianko, A.P., Nguyen, D.T., Doi, N.G., Roberts, R.G., 2019. The Pleistocene geoarchaeology and geochronology of Con Moong Cave, North Vietnam: site formation processes and hominin activity in the humid tropics. Geoarchaeology. https://doi.org/10.1002/gea.21758.
Michab, M., Feathers, J.K., Joron, J.L., Mercier, N., Selo, M., Valladas, H., Valladas, G., Reyss, J.L., Roosevelt, A.C., 1998. Luminescence dates for the paleoindian site of Pedra Pintada, Brazil. Quat. Sci. Rev. 17, 1041–1046. https://doi.org/10.1016/S0277-3791(97)00091-7.
Motta, J.A.O., org, 2003. Projeto cavernas de Mambaí: caracterização do ecossistema cárstico localizado no município de Mambaí e entorno. Brasília.
Murray, A.S., Wintle, A.G., 2000. Luminescence dating of quartz using an improved single- aliquot regenerative-dose protocol. Radiat. Meas. 32, 57–73.
Novello, V.F., Cruz, F.W., McGlue, M.M., Wong, C.I., Ward, B.M., Vuille, M., Santos, R.A., Jaqueto, P., Pessenda, L.C.R., Atorre, T., Ribeiro, L.M.A.L., Karmann, I., Barreto, E.S., Cheng, H., Edwards, R.L., Paula, M.S., Scholz, D., 2019. Vegetation and environmental changes in tropical South America from the last glacial to the Holocene documented by multiple cave sediment proxies. Earth Planet Sci. Lett. 524, 1–11. https://doi.org/10.1016/j.epsl.2019.115717.
Nunes, J.G. da S., Uagoda, R., n.d. Mapeamento de solos em área cárstica, através do estudo da catena com auxílio de geotecnologias e descrições em campo: Um estudo de caso na APA Nascentes do Rio vermelho, Mambaí – GO. Unpublished results.
Oliveira, P.V., Ribeiro, A.M., Oliveira, É.V., Viana, M.S.S., 2014. The dasypodidae (mammalia, xenarthra) from the urso fóssil cave (quaternary), parque nacional de ubajara, state of ceará, Brazil: paleoecological and taxonomic aspects. An. Acad. Bras. Cienc. 86, 147–158. https://doi.org/10.1590/0001-3765201420120029.
Osborne, R.A.L., 1986. Sedimentation in Caves- a Review, vol. 2. Publications of the Geological Society of Australia, pp. 189–217.
Osborne, R.A., 2005. Dating ancient caves and related palaeokarst. Acta Carsol. 34, 51–72.
Peyre, E., Guérin, C., Guidon, N., Coppens, Y., 1998. Des restes humains pléistocènes dans la grotte du Garrincho, Piauí, Brésil. Comptes Rendus de l'Academie des Sciences, Serie II. Sciences de la Terre et des Planetes 327, 335–360.
Piló, L.B., Auler, A.S., Neves, W.A., Wang, X., Cheng, H., Edwards, R.L., 2005. Geochronology, sediment provenance, and fossil emplacement at Sumidouro Cave, a classic Late Pleistocene/Early Holocene paleoanthropological site in eastern Brazil. Geoarchaeology 20, 751–764. https://doi.org/10.1002/gea.20081.
Plotnick, R.E., Kenig, F., Scott, A.C., 2015. Using the voids to fill the gaps: caves, time, and stratigraphy, 404. Geological Society Special Publication, pp. 233–250. https://doi.org/10.1144/SP404.5.
Prescott, J.R., Stephan, L.G., 1982. The contribution of cosmic radiation to the environmental dose for thermoluminescence dating. PACT 6, 17–25.
Rhodes, E.J., 2011. Optically stimulated luminescence dating of sediments over the past 200,000 years. Annu. Rev. Earth Planet Sci. 39, 461–488. https://doi.org/10.1146/annurev-earth-040610-133425.
Rizzato, P.P., Bichuette, M.E., 2014. Ituglanis boticario, a new troglomorphic catfish (Teleostei: Siluriformes: Trichomycteridae) from Mambaí karst area, central Brazil. Zool. 31, 577–598. https://doi.org/10.1590/s1984-46702014000600006.
Roosevelt, A.C., Costa, M.L., Machado, C.L., Michab, M., Mercier, N., Valladas, H., Feathers, J., Barnett, W., Silveira, M.I., Henderson, A., Sliva, J., Chernoff, B., Reese, D.S., Holman, J.A., Toth, N., Schick, K., 1996. Paleoindian cave dwellers in the Amazon : the peopling of the Americas. Science 272, 373–384.
Santos, G.M., Bird, M.I., Parenti, F., Fifield, L.K., Guidon, N., Hausladen, P.A., 2003. A revised chronology of the lowest occupation layer of Pedra Furada rock shelter, Piauí, Brazil: the Pleistocene peopling of the Americas. Quat. Sci. Rev. 22, 2303–2310. https://doi.org/10.1016/S0277-3791(03)00205-1.
SBE, UPE, GREGO, UFSCar, LES, 2014. Caracterização ambiental e conservação do sistema cárstico da gruna da Tarimba – Mambaí, GO. Report.
Springer, G.S., 2005. Clastic sediments in caves. In: Culver, David C., White, W.B. (Eds.), Encyclopedia of Caves. Elsevier Academic Press, San Diego, pp. 102–108.
Stríkis, N.M., 2015. Atividade do Sistema de Monção Sul-americana na porção central do Brasil durante o último período glacial a partir da aplicação de isótopos de oxigênio em espeleotemas.
Uagoda, R., Hussain, Y., Ferreira, C.F., Fonseca, M.R., Nogueira, A., Caldeira, D., Tavares, A., Nunes, J.G., Costa, B., 2019. In: Regional Conference of Geomorphology. Geomorphic Units Mapping of Fluviokarst Landscapes in Central Brazilian Higland, Athens, p. 212.
White, W.B., 2007. Cave sediments and paleoclimate. J. Cave Karst Stud. 69, 76–93.
Woodward, J.C., Goldberg, P., 2001. The sedimentary records in Mediterranean rockshelters and caves: archives of environmental change. Geoarchaeol. Int. J. 16, 327–354. https://doi.org/10.1002/gea.1007.